MYC disrupts transcriptional and metabolic circadian oscillations in cancer and promotes enhanced biosynthesis

Rachel E. DeRollo [1,*], Juliana Cazarin [1,*], Siti Noor Ain Binti Ahmad Shahidan [1], Jamison B. Burchett [1], Daniel Mwangi [1], Saikumari Krishnaiah [3,4,5], Annie L. Hsieh [6], Zandra E. Walton [6], Rebekah Brooks [6], Stephano S. Mello [1,2], Aalim M. Weljie [3,4,5,§], Chi V. Dang [7,8,9,§], and Brian J. Altman [1,2,§]

* These authors contributed equally

§ Co-corresponding authors

Lead contact: Brian J. Altman, Brian_Altman@urmc.rochester.edu

Aalim M. Weljie: aalim@pennmedicine.upenn.edu

Chi V. Dang: cvdang@jhmi.edu

Affiliations

1. Department of Biomedical Genetics, University of Rochester School of Medicine and Dentistry, Rochester, NY, USA
2. Wilmot Cancer Institute, University of Rochester Medical Center, Rochester, NY, USA
3. Department of Systems Pharmacology and Translational Therapeutics, Perelman School of Medicine, University of Pennsylvania, Philadelphia, PA, USA
4. Institute of Translational Medicine and Therapeutics, University of Pennsylvania, Philadelphia, PA, USA
5. Chronobiology and Sleep Institute, University of Pennsylvania, Philadelphia, PA, USA
6. The Wistar Institute, Philadelphia, PA, USA
7. Ludwig Institute for Cancer Research, New York, NY, USA
8. Department of Oncology, Johns Hopkins University, Baltimore, MD, USA
9. Department of Biochemistry and Molecular Biology, Johns Hopkins University, Baltimore, MD, USA

Abstract

The molecular circadian clock, which controls rhythmic 24-hour oscillation of genes, proteins, and metabolites, is disrupted across many human cancers. Deregulated expression of MYC oncoprotein has been shown to alter expression of molecular clock genes, leading to a disruption of molecular clock oscillation across cancer types. It remains unclear what benefit cancer cells gain from suppressing clock oscillation, and how this loss of molecular clock oscillation impacts global gene expression and metabolism in cancer. We hypothesized that MYC suppresses oscillation of gene expression and metabolism to instead upregulate pathways involved in biosynthesis in a static, non-oscillatory fashion. To test this, cells from distinct cancer types with inducible MYC or the closely related N-MYC were examined, using detailed time-series RNA-sequencing and metabolomics, to determine the extent to which MYC activation disrupts global oscillation of genes, gene expression, programs, and metabolites. We focused our analyses on genes, pathways, and metabolites that changed in common across multiple cancer cell line models. We report here that MYC disrupted over 85% of oscillating genes, while instead promoting enhanced ribosomal and mitochondrial biogenesis and suppressed cell attachment pathways. Notably, when MYC is activated, biosynthetic programs that were formerly circadian flipped to being upregulated in an oscillation-free manner. Further, activation of MYC ablates the oscillation of nutrient transporter glycosylation while greatly upregulating transporter expression, cell surface localization, and intracellular amino acid pools. Finally, we report that MYC disrupts metabolite oscillations and the temporal segregation of amino acid metabolism from nucleotide metabolism. Our results demonstrate that MYC disruption of the molecular circadian clock releases metabolic and biosynthetic processes from circadian control, which may provide a distinct advantage to cancer cells.

Introduction

Circadian rhythms are ~24-hour rhythms that occur in many organisms and can be observed on the cellular level to rhythmically control transcription, protein levels, and metabolic processes. Recent analyses have revealed that human cancers have consistently disrupted or ablated circadian clocks. However, what impact circadian disruption has on cancer cell transcriptional and metabolic programming has not been determined.

Circadian rhythms entrain organisms' activity (such as sleep-wake cycles) and metabolism (such as segmentation of catabolism and biosynthesis) to the day / night cycle. The 'central clock', housed within the suprachiasmatic nucleus of the hypothalamus, receives light signals through the eye and communicates these signals to peripheral cell-autonomous 'molecular clocks' present in every cell and tissue, which control oscillatory gene expression [1]. The molecular clock is controlled by the basic helix-loop-helix (bHLH) transcription factors CLOCK and BMAL1, which, as a heterodimer, rhythmically regulate target gene expression in an oscillatory fashion [1]. CLOCK and BMAL1 control their own activity and levels through a series of feedback loops. In the first and most central loop, rhythmically produced PER and CRY proteins inhibit the activity of CLOCK and BMAL1, leading to antiphase oscillation of CLOCK-BMAL1 activity and PER and CRY levels and localization. In a second loop required for molecular clock function in many cells and tissues, the nuclear hormone receptors and transcriptional repressors REV-ERBα and REV-ERBβ compete with the transcriptional ROR activators to rhythmically control transcription of BMAL1 (*ARNTL*) ([1-3]). The molecular clock is thus responsible for the rhythmic regulation of thousands of transcripts in mouse and primate, comprising more than 50% of protein coding transcripts in some tissues [4, 5]. Oscillatory gene expression arises from direct action of CLOCK-BMAL1 on promoters and enhancers, from binding of the REV-ERB and ROR family to promoters, and from action of secondary tissue-specific transcription factors that themselves are rhythmically controlled by the molecular clock [6, 7]. Importantly, not all oscillation in a cell arises solely from mRNA: several studies have shown that proteins and metabolites also oscillate in a manner not directly dependent on mRNA oscillation [8-10].

The molecular circadian clock is tumor suppressive in many tissues. Indeed, disruption of the molecular clock, either by behavioral disruption or genetic mutation, can accelerate or initiate

tumorigenesis in lung, liver, bone, colon, melanocyte, and other cell types [11-19]. Supporting the notion that the clock is tumor suppressive in human cancer, circadian gene expression is often disrupted in tumor tissue as compared to normal tissue [20]. Perhaps more importantly, three independent computational analyses each revealed that normal progression and oscillation of the circadian clock is dampened or lost in human tumor tissue compared to normal tissue [21-23]. We and others have proposed that clock disruption in cancer may release cellular processes such as cell cycle or metabolic fluxes from circadian control to be constantly and statically up- or downregulated [24, 25]. However, given that mutations in molecular clock genes are rare [26], it remains unclear how circadian disruption arises in cancer cells, and what formerly circadian programs lose oscillation as a result of this disruption.

A well-defined source of circadian disruption in cancer is amplification of the *MYC* oncogene or its closely related paralogue *MYCN* (N-MYC), which leads to overexpression of MYC or N-MYC. Amplification of at least one *MYC* family member is quite common in human cancer, overall occurring in nearly one third of all cases [27]. The MYC-family proteins are E-box binding transcription factors which, when amplified, have also been proposed to increase overall transcriptional output [28, 29]. When MYC is amplified, it tends to drive continued transit through the cell cycle, and to upregulate nutrient uptake, protein translation, and biomass accumulation, amongst many other functions [27, 28, 30] Amplified MYC and N-MYC have been shown in multiple cancer models to dampen or ablate molecular clock gene oscillation [31-36]. We identified a mechanism whereby MYC and N-MYC directly upregulate the REV-ERB proteins, leading to BMAL1 suppression and a collapse of molecular clock gene oscillation [31, 32]. We also observed that cell-autonomous oscillation of glucose was disrupted by MYC [32]; however, it remained unclear which global transcriptional and metabolic programs that are normally circadian controlled were disrupted by MYC amplification. Since MYC drives enhanced nutrient uptake and biosynthesis across multiple cancer, we hypothesized that MYC disruption of the molecular clock releases these processes from circadian control to instead be enhanced by amplified MYC.

In this study, we utilize multiple cell line models representing neuroblastoma and osteosarcoma to determine the role of MYC overexpression in disruption of circadian oscillations of transcription and cell-autonomous metabolism. We perform time-series analysis to identify which transcriptional programs are

circadian in the absence of MYC across multiple cell lines; and also determine, in a time-independent fashion, which genes and pathways MYC upregulates or suppresses in common between the three cell models. We next combine these two analyses to determine which of gene expression programs and pathways switch from being oscillatory to being up- or downregulated when MYC is activated. In our analysis, we have taken an agnostic approach, presenting the most significantly enriched genes and pathways rather than choosing specific pathways of interest. Using this agnostic approach, we determine that across multiple cell lines, pathways associated with metabolism and biosynthesis lose oscillation and become upregulated by MYC in a static, oscillation-independent fashion. Finally, we examine which metabolic circadian cycles are disrupted by MYC, and how these connect to changes in the oscillation and expression of nutrient transporters.

Results

Oncogenic MYC ablates global transcriptional oscillation

We and others have shown that ectopic MYC disrupts the molecular clock machinery across many types of cancer models [31-36]. Since many of the components of the molecular clock pathway, including CLOCK, BMAL1, and the REV-ERB proteins are transcription factors, it can be surmised that disruption in normal oscillation of the molecular clock may lead to loss of rhythmicity of global circadian output. Similarly, MYC may upregulate genes and programs formerly regulated by the molecular clock. Therefore, the global transcriptional impact of loss of molecular clock gene expression rhythmicity remained unclear. To address this, we utilized three separate cancer cell lines we previously characterized to have intact molecular clocks that are disrupted by overexpressed MYC or N-MYC: SHEP N-MYC-ER (neuroblastoma), SKNAS N-MYC-ER (neuroblastoma), and U2OS MYC-ER (osteosarcoma) [31, 32]. All three lines have inducible overexpressed MYC-ER or N-MYC-ER that is activated by 4-hydroxytamoxifen (4OHT). Activated MYC-ER and N-MYC-ER will henceforth be referred to for all cell lines as MYC-ON. When overexpressed MYC-ER is inactive in control conditions, this condition is referred to as MYC-OFF. We performed time-series analysis on these three cell lines ± MYC activation: cells were entrained with dexamethasone at CT0, and collected from CT24-72 or 76 at 2-4 hour intervals. CT refers to ‘circadian time’, the number of hours after

dexamethasone entrainment. In all three lines, MYC activation dampened or ablated oscillation of *PER2, NR1D1* (REV-ERBα), and *ARNTL* (BMAL1) (**Figure 1A**, SKNAS data published previously in [31, 32]). We next performed RNA-sequencing of each cell line and time series ± MYC activation, and used the ECHO algorithm [37] to detect oscillating genes. Depending on cell line, we detected between ~700-1600 oscillating genes in the MYC-OFF condition. Supporting the notion that the identity of circadian output genes is highly variable between different cell and organ systems [4, 5], there was little overlap in the specific identity of oscillating genes in the MYC-OFF conditions amongst the three cell lines (**Supplemental Figure S1A**). Nonetheless, when we examined these oscillatory genes in the MYC-ON condition, we found that nearly 90% of genes that oscillated in MYC-OFF no longer oscillated in MYC-ON (**Figure 1B**). This suggested a global collapse of the normal transcriptional oscillatory program in the presence of ectopic MYC.

Surprisingly, when MYC was activated, many genes gained oscillation that were previously not oscillatory. We found that MYC-ON cells contained between ~500-1500 oscillating genes, with approximately 90% not oscillating in MYC-OFF (**Supplemental Figure 1B**). MYC suppresses BMAL1 expression (**Figure 1A and [31-34]**), and it was previously suggested that oscillations occurring in low or absent BMAL1 may be of very low amplitude [38, 39]. To test whether this was occurring in our cell line models, we examined the amplitude of all genes oscillating with a circadian period in MYC-OFF and MYC-ON (**Supplemental Figure 1C**). We found no particular tendency of oscillating genes to be of lower amplitude in MYC-ON across all three cell lines. Overall, these results showed that activation of ectopic MYC suppressed normal circadian oscillatory output across multiple independent models.

Oncogenic MYC causes a shift in the number and identity of oscillating transcriptional programs

While the individual identity of oscillating genes varies widely between tissues, there are basic cellular functions that are nonetheless commonly circadian-regulated across multiple tissues and cell types [4, 5]. For instance, it was shown in baboon that metabolic, vesicle-trafficking, and cell membrane and junction gene expression programs are commonly rhythmic in many different tissues [5]. Given the lack of overlap in the specific identity of oscillating genes in our three cell line models in MYC-OFF conditions, we next

asked which transcriptional programs oscillated in each of these cells. To accomplish this, we used complementary methods of phase-dependent and phase-independent analysis. Phase-dependent analysis assumes that mRNAs in a given pathway or group peak together in the same circadian phase, and thus groups genes that peak together for pathway analysis. We used the phase-dependent algorithm Phase Set Enrichment Analysis (PSEA) to determine which gene sets and pathways were enriched in oscillating genes in MYC-OFF and MYC-ON in a phase-dependent fashion [40]. To determine when these programs peaked, we plotted significantly enriched oscillating programs on radial histograms, which circularize the X-axis to accurately show a repeating circadian time scale of CTs. Similar to individual genes in **Figure 1**, most of the enriched oscillatory programs in MYC-OFF did not oscillate in MYC-ON (**Figure 2A**). Intriguingly, even when oscillation was maintained from MYC-OFF to MYC-ON, the time in which these programs peaked was altered. For instance, in SHEP MYC-OFF, most gene expression programs detected peaked between CT 17-21, while in MYC-ON, those that were shared instead peaked mostly between CT 6-15. Similar to SHEP, SKNAS neuroblastoma had a majority of oscillating programs peak at CT 18 in MYC-OFF (with a smaller portion peaking at CT 5), which in MYC-ON, the few remaining oscillatory programs peaked at CT 4 and 17. U2OS osteosarcoma were also similar to the two neuroblastoma lines: in MYC-OFF, the strongest peak occurred at CT16, while no shared gene sets peaked at this time in MYC-ON. The gene sets determined as being oscillatory in MYC-ON also had different timing of peak expression compared to MYC-OFF (**Supplemental Figure 2A, compare to Figure 2A**). We focused on which gene expression programs were shared by at least two cell lines and ranked these according to average significance score across the cell lines. Similar to previous findings in baboon, in MYC-OFF cells, those shared between cell lines corresponded to cytoskeleton, endoplasmic reticulum, cell junction and contact, and metabolism and biosynthesis (particularly in those sets shared between the neuroblastoma cell lines SHEP and SKNAS) (**Figure 2B**). In contrast, there was far less overlap of oscillating gene expression programs in MYC-ON (**Supplemental Figure 2B**), and no identifiable common themes emerged. This suggested MYC does not drive a common oscillatory program at the transcript level in different cell lines.

We also utilized a phase-independent analysis methodology to determine which transcriptional programs were enriched amongst oscillatory genes. Some oscillatory programs, including cell cycle and the molecular circadian clock itself, have genes that peak at different times of the day [41, 42], making detection of these programs with PSEA inefficient. Thus, we analyzed oscillatory genes in each cell line regardless of their peak of oscillation for pathway enrichment with ToppFun functional enrichment suite, which combines several different enrichment libraries [43]. We found that, despite the fact that there were largely similar numbers of oscillating genes between MYC-OFF and MYC-ON, there tended to be less enriched gene sets among MYC-ON. In SHEP MYC-OFF, oscillating genes were enriched for endosomal and lysosomal trafficking, in U2OS, programs related to the molecular circadian clock were enriched, and in SKNAS, a program related to toll-like receptor signaling was enriched (**Table 1**). In contrast, in SHEP and U2OS MYC-ON, programs related to cell cycle were instead enriched, while no programs were significantly enriched in SKNAS MYC-ON (**Table 1**).

We further investigated this apparent gain in cell cycle gene rhythmicity in SHEP and U2OS MYC-ON by interrogating which cell cycle genes were oscillatory with a ~24-hour period in the absence or presence of activated MYC. In both cell lines, there were fewer significantly rhythmic cell cycle genes in MYC-OFF (11 in SHEP, 3 in U2OS) as compared to MYC-ON (16 in SHEP, 5 in U2OS, **Supplemental Figure 2C,D**), suggesting a potential gain in cell cycle gene oscillation in the presence of MYC as circadian rhythmicity is diminished. This agrees with prior findings in U2OS that intentional disruption of the molecular clock promotes enhanced cell cycle advance [17]. Overall, these data suggested that ectopic MYC reduces or abrogates rhythmicity of gene expression programs that normally are controlled by the molecular clock, and instead may promote cell cycle rhythmicity.

Oncogenic MYC promotes a distinct program of biosynthesis and loss of attachment across multiple cell models

We next sought to address which genes and pathways MYC up- or downregulated without regards to rhythmicity. MYC can have many disparate functions in cancer, which may depend on 1) the degree to which MYC is overexpressed, 2) which promoters and enhancers it binds, 3) if MYC cooperates with other

transcription factors such as MIZ1 to inhibit expression of certain genes, and 4) if MYC strongly regulates pause release ([27, 29, 44-47]. Our MYC-ER models gave us the opportunity to determine the role of MYC activation across three unrelated cell lines, and to determine commonalities in MYC rewiring global transcription. To accomplish this, we performed differential expression analysis, using DeSeq2, on our time-series RNA-sequencing experiments [48]. Differential expression analysis revealed that MYC activation resulted in the upregulation (by a least 10%) between ~4500 to ~7700 genes and suppression (by at least 10%) between ~6000 to ~8000 genes (**Figure 3A**), in line with previous reports that MYC exerts a strong genome-wide repressive role [49, 50]. Overall, this corresponded to approximately 30-40% of all genes detected by RNA-sequencing. We performed Gene Set Enrichment Analysis (GSEA) for all genes up- or down-regulated by at least 10%, and observed which gene sets were enriched in common between all three cell lines [51-54]. There were 172 gene sets upregulated in common between the three inducible cell lines. Common programs were focused on canonical MYC targets, mitochondrial gene expression and assembly, ribosome biogenesis, tRNA processing, and metabolism (**Figure 3B**). In contrast, 303 gene sets were downregulated in common between all three cell lines. These suppressed gene expression programs corresponded to cell adhesion, extracellular matrix (ECM), collagen, and focal adhesion (**Figure 3C**), consistent with previous reports that MYC may promote an invasive and metastatic phenotype in cancer cells [55-57].

We next asked if these changes in gene expression were represented only in genes strongly up- or down-regulated by MYC. GSEA can detect small differences across many genes [51], so we sought to confirm that these programs arose from highly upregulated or downregulated genes by performing a second independent analysis of differential expression using a different functional enrichment platform, ToppFun [43]. We focused on genes that were at least 1.5-fold up- or down-regulated (**Supplemental Figure 3A**), and found that the three cell lines had 687 genes upregulated 1.5-fold in common, and 802 genes downregulated 1.5 fold in common (**Supplemental Figure 3B,C**). We subjected each of these in-common gene sets to ToppFun pathway enrichment analysis, and obtained highly similar results to GSEA analysis. Upregulated programs included mitochondrial and ribosomal biogenesis (**Supplemental Figure 3D**), while downregulated programs included those related to ECM, collagen, and focal adhesion

(**Supplemental Figure 3E**). These results suggested strong commonalities in the MYC-driven transcriptional program between three unrelated cell lines representing two different forms of cancer.

Oncogenic MYC impairs oscillatory gene expression to drive static gene expression programs.

Given that MYC disrupts normal molecular circadian clock rhythmicity across multiple systems, a key question arises: which oscillatory programs are shifted by MYC from being oscillatory in MYC-OFF to being statically up- or down-regulated when MYC is activated? The answer to this question would explain how MYC shifts the behavior of cells by disrupting their molecular clock and circadian rhythmicity, and begin to explain what benefit MYC-amplified cancers gain from disruption of the molecular circadian clock. We asked this question both at the pathway-level and at the gene-level using complementary methodologies. At the pathway-level, we first determined which gene expression programs were oscillatory in MYC-OFF cells, as determined by PSEA (as discussed in **Figure 2**), lost oscillation when MYC was turned on. We then examined overlap between these programs that lost oscillation and which programs were determined to be up- or down-regulated by MYC via GSEA analysis (see schematic in **Figure 4A**). In both SHEP and SKNAS, programs that lost oscillation and became upregulated corresponded to ribosomal biogenesis, mitochondria, RNA splicing, and metabolism (**Figures 4B-C**). This was similar to those programs that were upregulated by MYC in these cells (see **Figure 3B** and **Supplemental Figure 3B**). Those programs that switched from being oscillatory to downregulated corresponded to ER, lysosome, and aging in SHEP, and morphology and synaptic membranes in SKNAS (**Figures 4B-C**). These gene sets were less similar to those downregulated by MYC in these cell lines (see **Figure 3C** and **Supplemental Figure 3C**). Conversely, we did not detect in U2OS overlap between oscillating programs and those that became up or down-regulated (not shown), suggesting that disruption of oscillation in U2OS may occur more at the protein or metabolite level.

We cross-validated these results with an independent approach that focused on the gene level (**Supplemental Figure 4**). In this approach, we first identified genes that had significant circadian oscillation in MYC-OFF, as identified in ECHO, and lost this oscillation in MYC-ON (see **Figure 1**). Of these genes that lost oscillation in MYC-ON, we next asked which were significantly up- or down-regulated

by MYC, using DeSeq2, and finally queried these overlapping genes for gene set enrichment by ToppFun (see schematic in **Supplemental Figure 4A**). In SHEP and SKNAS, programs corresponding to genes that switched from being oscillatory to upregulated were similar to those determined by PSEA and GSEA in **Figure 4**, corresponding to ribosome assembly, mitochondrial activity, and protein translation (**Supplemental Figure 4A,B**). In contrast in U2OS, upregulated programs mostly corresponded to the molecular clock itself as well as macromolecular protein complex programs (**Supplemental Figure 4C**). There were comparatively fewer downregulated programs that were identified with this approach: in SHEP, the few downregulated programs corresponded to cell adhesion and organization, while in U2OS the downregulated programs corresponded to circadian rhythm and cell organization; there were no detected downregulated programs in SKNAS (**not shown**). Overall, these results suggested that, across multiple cancer models, MYC disrupts circadian transcriptional oscillation and instead promotes static (non-oscillatory) regulation of processes such as biosynthesis, metabolism, and extracellular matrix-related gene expression programs.

Rhythmic glycosylation and expression of nutrient transporters are disrupted by MYC.

Intracellular metabolism is known to be highly circadian [10, 58-60], potentially balancing anabolic and catabolic metabolism in concert with whole body rhythms. In contrast, cancer cells, particularly those driven by MYC, engage in upregulated nutrient uptake and biosynthesis [28, 61]. Our data indicated that in multiple cell lines, MYC caused metabolic and biosynthetic processes that were formerly circadian to flip to static upregulation (**Figure 4, Supplemental Figure 4**). In addition, we have previously observed that MYC expression in U2OS ablated oscillation of intracellular glucose while boosting uptake of glucose and glutamine [31]. Since these processes are regulated in part by nutrient transporter expression and availability, we asked whether nutrient transporter rhythmicity and expression is affected by MYC in three cell models. We focused on the two subunits of the LAT1 amino acid transporter: LAT1 (*SLC7A5)* and 4F2hc (*SLC3A2*, also known as CD98), which transport glutamine and other amino acids, as well as the ubiquitously expressed GLUT1 glucose transporter (*SLC2A1*) [62-64]. GLUT1 and 4F2hc are glycosylated, which aids in their trafficking to the plasma membrane [65, 66], so we performed immunoblot using a

technique to determine glycosylation level of these proteins [66]. Where appropriate, two different exposures of the same immunoblot ('dark' and 'light') are shown. In all three cell lines, glycosylated 4F2hc and total levels of LAT1 showed periodic expression in MYC-OFF (**Figure 5A-C**). In contrast, when MYC was activated, oscillation of LAT1 and rhythmic glycosylation 4F2hc was lost, but total glycosylation of 4F2hc and total levels of each of these proteins were greatly increased (**Figure 5A-C**). In U2OS in MYC-OFF conditions, GLUT1 also showed oscillatory glycosylation, while when MYC was activated, this oscillation was lost and GLUT1 glycosylation was increased (**Figure 5A**). In SHEP cells, GLUT1 glycosylation was not oscillatory in MYC-OFF but was still increased by MYC expression (**Figure 5B**), while in SKNAS, glycosylated GLUT1 was not regulated by MYC (**Figure 5C**). For 4F2hc and GLUT1 we treated some samples with PNGase-F, a glycosidase [66], to demonstrate which bands were glycosylated protein and to compare total levels of protein in the presence or absence of MYC. We found that total levels of 4F2hc were increased by MYC in all three cell lines, while in contrast, total GLUT1 levels were not increased by MYC (**Figures 5A-C**), suggesting that MYC regulated glycosylation but not expression of GLUT1 in U2OS and SHEP. We also observed that MYC did not alter mRNA levels of GLUT1 *(SLC2A1,* **not shown**), in contrast to previous reports that MYC transcriptionally upregulates *SLC2A1* in other cancer models [67]. As has been shown previously [31, 32], we also observed suppression of BMAL1 and upregulation of REV-ERBα regardless of timepoint (**Figures 5A-C**). Overall, these data suggested that nutrient transporter expression and glycosylation is rhythmically regulated and ablated by MYC, as MYC increases post-transcriptional modification and levels of these transporters.

The above findings on nutrient transporter glycosylation did not demonstrate whether these transporters were actually reaching the cell surface, whether cell surface expression of transporters was increased by MYC, and whether these resulted in identifiable metabolic changes in the cells. To address this, we performed an On-cell Western [68], which stains fixed and unpermeabilized cells in a dish to determine surface expression of a target protein. We focused on LAT1, and found that surface expression of LAT1 was significantly increased in MYC-ON as compared to MYC-OFF cells (**5D-E**), suggesting that an increase in expression and glycosylation correlates with more transporter on the cell surface. To further determine whether changes in nutrient transporter expression, glycosylation, and localization correlated

with increases in intracellular metabolite pools, we performed ultra-performance liquid chromatography-tandem mass spectrometry (UPLC-MS/MS) metabolomics in U2OS, in the presence or absence of activated MYC. In two independent experiments, we found that almost all amino acids were significantly increased in MYC-ON (**Figure 5F, Supplemental Figure 5**), suggesting that increased nutrient transporter expression and glycosylation correlated with enhanced intracellular amino acid pools. Overall, these data showed that MYC ablates nutrient transporter oscillation and increases transporter expression, cell surface localization, and activity.

MYC disrupts metabolic circadian oscillations in a cell-autonomous manner

The ablation of oscillatory nutrient transporter glycosylation and expression, along with our previous analysis of metabolic oscillations by NMR and mass spectrometry [10, 31], raised the intriguing possibility that MYC may disrupt global cell-autonomous metabolic oscillation. To test this, we performed time-series metabolomic analysis using UPLC-MS/MS at 2-hour intervals in dexamethasone-entrained U2OS MYC-ER cells over two independent experiments, termed Replicate A and Replicate B. Using the ECHO algorithm, we found in Replicate A that there were 37 oscillating metabolites in MYC-OFF, while only 6 of these metabolites remained oscillatory with a ~24-hour period in MYC-ON (**Figure 6A**)**.** The traces of individual metabolites were plotted for MYC-OFF and MYC-ON in **Figure 6B**. Similar results were observed in Replicate B (**Supplemental Figure 6A-B**). In concordance with our transcriptomic observations, some metabolites in both Replicates gained 24-hour rhythmicity in MYC-ON that did not previously have this rhythmicity in MYC-OFF (**Supplemental Figure 6C-D**).

Finally, we queried which metabolic programs were circadian in MYC-OFF and MYC-ON by performing KEGG enrichment analysis. Peak phase of metabolites was determined, KEGG analysis was performed separately on each set of oscillating metabolites, and the resulting significantly enriched pathways were plotted in polar histograms. In both Replicates A and B for MYC-OFF, we observed peaks of oscillation at CT10 and CT20. Those at CT10 corresponded to programs in nucleotide metabolism, while those at ZT20 instead were enriched for programs in amino acid metabolism and tRNA biosynthesis (**Figure 6C and Supplemental Figure 7A**). In contrast, there was no discernable pattern in MYC-ON

cells: in Replicate A, metabolic programs were clustered around a single timepoint, while in Replicate B, they were fragmented in a manner distinct from MYC-OFF (**Figure 6C, Supplemental Figure 7B**). These observations demonstrate that cells without amplified ectopic MYC engage in circadian oscillatory metabolism that temporally separates different bioenergetic processes, which is disrupted when MYC is elevated and active.

Discussion

We and others previously showed that MYC disrupts molecular clock oscillation in cancer cells, but the reasons for this, and what specific benefit cancer cells might gain, remained unclear. Our findings, in sum, indicate that overexpressed MYC suppresses circadian oscillation of transcriptional and metabolic programs across multiple models of cancer (**Figure 7**). MYC overexpression led to a greater than 85% loss of global transcriptional oscillation in neuroblastoma and osteosarcoma cell lines. To identify robust signatures of which genes were circadian in MYC-OFF (low-MYC) cell lines, and which genes were regulated by MYC in MYC-ON (overexpressed MYC) cell lines, we focused only on genes and pathways that overlapped between at least two of the three cell lines in our study. In the absence of overexpressed MYC, we found that oscillating genes which overlapped between multiple cell lines were enriched for pathways associated with metabolism, biosynthesis, endoplasmic reticulum, extracellular matrix and adhesion. In contrast, when MYC was activated, we found that MYC upregulated genes associated with metabolism and biosynthesis, and suppressed genes associated with adhesion and extracellular matrix. More importantly, we identified, for the first time, that genes and pathways that oscillate in the absence of overexpressed MYC lose oscillation when MYC is activated and become instead up- or down-regulated. Notably, metabolic and biosynthetic processes were most significantly enriched in pathways and genes that shifted from oscillatory in MYC-OFF to upregulated in MYC-ON. These results indicated that cells with oncogenic MYC release metabolism from circadian control, instead upregulating metabolic gene expression programs without regards to oscillation. Further focusing on metabolism, we found that nutrient transporters demonstrate oscillatory glycosylation, associated with membrane localization, and this rhythmic oscillation of nutrient transporter glycosylation and expression is ablated by MYC as MYC

massively upregulated glycosylated nutrient transporters across multiple cell lines. Finally, oscillation of metabolites themselves were also suppressed by MYC, and circadian segregation of anabolic and catabolic metabolic processes was ablated. Overall, our findings for the first time show MYC suppresses oscillation of genes associated with metabolism and biosynthesis to instead upregulate these processes and engage in heightened metabolism in an oscillation-independent fashion.

Our findings that MYC shifts certain metabolic and cell-attachment pathways from being oscillatory to being up- or down-regulated is supported by observations of similar phenomena from human cancer samples. It has historically been difficult to assess the state of the molecular circadian clock in human tumor samples since these samples are from single timepoints, and time of day information is often unavailable. However, several recent studies using distinct methodologies have all determined that rhythmicity tends to be dampened or ablated in human tumors compared to normal tissue [21-23, 69]. One weakness of these techniques is that, currently, they cannot detect phase or period changes in oscillation, only amplitude changes. Nonetheless, in addition to identifying lost rhythmicity of the molecular clock in tumors, these studies interrogated which pathways had decreased oscillation in tumors. One study, using a methodology known as LTM (Lunch Table Method), found across 11 tumor types that the pathways most associated with circadian rhythmicity in tumors were those related to extracellular matrix, collagen, and TCA cycle and electron transport (metabolism) [69]. In our study, we observed that these same pathways in MYC-ON cells were among the ones most likely to lose oscillation and become upregulated (metabolism) or suppressed (ECM and collagen). The authors of the LTM study speculated that the correlation between ECM / collagen rhythmicity and tumor rhythmicity may be related to cellularity of the tumor (ie, tumors with more endothelial and fibroblast cells have less cancer cells and more rhythmicity) [69], whereas our findings suggest a possible tumor-cell autonomous mechanism for loss of ECM rhythmicity in cancer cells. A separate study, using a methodology known as CYCLOPS (cyclic ordering by periodic structure), found that pathways related to redox metabolism and hypoxia were dampened in hepatocellular carcinoma (HCC) compared to normal liver [21]. More intriguingly, the authors also identified GLUT2 (*SLC2A2*) as a transcript that displayed dampened oscillation in HCC compared to normal liver and kidney. These findings are similar to our observations that MYC upregulates and ablates

oscillation of metabolic pathways and nutrient transporters across multiple cancer types. The Authors of the CYCLOPS study did not identify a mechanism for this loss of oscillation, but since HCC is known to be driven by amplified MYC [70], it is possible to speculate that elevated and deregulated MYC in HCC may drive this loss of rhythmicity in metabolic processes. Overall, our findings for the first time provide a potential mechanism for the loss of oscillating pathways and metabolic processes in cancer cells.

MYC is often overexpressed in cancer, and in many cases, this overexpression arises from either genomic translocation or amplification events, which occur in at least 28% of all human cancers [27]. The MYC-ER and N-MYC-ER systems model genomic amplification in cancer, where MYC is no longer under the control of endogenous promoter and other regulatory elements [71]. In these cancer models where MYC is amplified, we and others have shown that MYC suppresses or interferes with BMAL1 and disrupts molecular clock oscillation [31-36]. Our results now show that when MYC disrupts the molecular clock, this is accompanied by widespread suppression of genetic and metabolic oscillations that occur in the absence of amplified MYC. More notably, our findings suggest that MYC “releases” biosynthetic and metabolic processes from circadian control in order to be upregulated without regards to oscillation. However, the molecular circadian clock is not disrupted in all cancers, and in particular seems to be maintained (albeit in an altered state) in those driven by mutated HRAS or KRAS [72-74]. In fact, alteration (but not complete ablation) of the circadian clock may enhance MYC expression even in cases where MYC is not amplified, and MYC itself is circadian-regulated and oscillatory in these settings [12, 17, 75-77]. In cancer models where MYC is upregulated (by another oncogene or through circadian disruption), and is potentially still circadian-controlled, MYC does not seem to exert a strong effect in suppressing BMAL1 and ablating rhythmicity of the molecular clock or downstream targets [11, 17, 75-77]. One notable exception is in glioblastoma stem cells (GSCs), where GSCs with amplified MYC maintained oscillation and actually relied on CLOCK and BMAL1 to maintain stemness [78]. A similar necessity for the circadian clock was seen in acute myeloid leukemia stem cells [79]. It may be that GSCs (and other select cancer stem cell populations) with amplified MYC specifically select for rare populations where clock function is somehow maintained. Nonetheless, in most cases from the literature, amplification of MYC results in severe clock

dysfunction, and our findings now suggest that MYC amplification result in a loss of rhythmicity in pathways related to biosynthesis and proliferation.

We observed that some genes and pathways gained oscillation when MYC was activated. Generally, far fewer pathways were enriched in MYC-ON oscillatory genes than MYC-OFF oscillatory genes, indicating some degree of stochasticity in which genes gained oscillation. One notable group of genes that gained oscillation were cell cycle-related genes, consistent with the notion that MYC induces cell cycle advance [30]. Interestingly, several recent papers reported that metabolic oscillations associate with active cell cycle, though there was not consensus on whether these oscillations depended on cell cycle progression [80, 81]. Thus, it is possible that the metabolic oscillations we observe in MYC-ON (**Figure 6, Supplemental Figures 6-7**) originate from cell cycle progression and not from the molecular clock. Nonetheless, the source of gene and metabolite oscillations in MYC-ON cells remains unclear. We note that while BMAL1 is suppressed by MYC, its expression is not ablated (**Figure 1** and [31-34, 36]). Thus, it is possible that these oscillations originate from residual CLOCK-BMAL1 activity. Indeed, we previously showed that MYC competes with BMAL1 for binding to the *NR1D1* (REV-ERBα) promoter [31]. We speculate that MYC, when amplified, may similarly compete for CLOCK-BMAL1 binding sites genome-wide, and oscillations that emerge in MYC-ON cells may arise from new sites occupied by CLOCK-BMAL1 in circumstances where MYC competes for their normal binding sites. A future line of inquiry should determine if non-canonical circadian oscillations that emerge in MYC-amplified cancer cells contribute to proliferation or metabolic phenotype.

Metabolic rewiring supports cancer cell proliferation and growth, and our findings suggest that loss of circadian oscillation by MYC may be a feature of metabolic rewiring. This rewiring relies not only on the aberrant expression and activity of enzymes from the glycolytic, oxidative, and biosynthetic pathways but also on optimizing the influx and efflux of nutrients by solute carrier proteins (SLCs) [61]. Notably, all these processes are regulated by oncogenic MYC [28, 82]. One example is the loss of rhythmicity we observed in the LAT1 amino acid transporter. LAT1 a heterodimeric transporter complex of LAT1 (*SLC7A5*) with 4F2hc (*SLC3A2*), which is required for LAT1 functional activity, stability, and proper location in the plasma membrane [62]. LAT1 is a key mediator of essential amino acid uptake, promoting amino acid

homeostasis and mTORC1 pathway activation in cancer cells, which supports cell proliferation and survival [83, 84]. The LAT1 subunit is upregulated in various cancers, while its inhibition reduces tumor growth [84, 85]. Our results show that MYC activation ablates oscillation and increases LAT1 total protein expression and membrane localization, corroborating previous findings of MYC-dependent upregulation of LAT1 [85-88]. MYC effects on LAT1 may rely on transcriptional mechanisms, since MYC binds to E-box regions in the LAT1 promoter [86]. LAT1 forms a heterodimeric transporter complex with 4F2hc, also a MYC target, which is required for LAT1 functional activity, stability, and proper location in the plasma membrane [62, 89, 90]. 4F2hc harbors four N-glycosylation sites that are required for proper stability and trafficking to the membrane. Mutation of those sites correlates with a lower abundance of LAT1 in the plasma membrane and reduced transport activity [65]. We found in our cancer cell modes that when MYC was activated, the rhythmicity of 4F2hc glycosylation was lost, and increased expression of glycosylated 4F2hc was detected in all three cell lines. The surface expression of LAT1 and intracellular amino acid pools were significantly increased in MYC-ON compared to MYC-OFF cells in U2OS cells, suggesting that MYC disrupts expression and glycosylation oscillations to drive static but highly active transporter states.

MYC has been shown to increase glycolytic flux in cancer cells by upregulating several glycolytic pathway enzymes, including hexokinase and LDH activity, and increasing GLUT1-mediated glucose uptake [67]. We previously found that U2OS cells lost intracellular glucose oscillation when MYC was activated [31], but the mechanism for this remained unclear. The glucose transporter GLUT1 was previously described to be transcriptionally regulated by MYC, and contributes to MYC-mediated increase in glycolytic flux in cancer cells [67, 91]. Interestingly, we did not observe an alteration in GLUT1 total mRNA or protein by MYC; however, GLUT1 glycosylation, which is required for its localization to the plasma membrane [66, 92], was increased in MYC-ON conditions in U2OS and SHEP cells. Alongside this, circadian oscillation of GLUT1 glycosylation was lost under MYC-ON compared to MYC-OFF condition in U2OS. These results corroborate previous findings showing MYC-dependent loss of circadian oscillation of hexokinase 2 protein expression and intracellular levels of glycolytic metabolites, including glucose, in U2OS cells [31]. Overall, our data bring new mechanistic insights into how MYC disrupts cell-autonomous metabolic oscillation,

454 which is driven by both suppressing the oscillatory expression of transporters and metabolic enzymes and
455 uncoupling the regulation of the sub-cellular trafficking of metabolite transporters from circadian control.

456 For the purposes of this study, we focused on the "top hits" from each of our analyses (PSEA,
457 GSEA, etc), and present them as ranked lists. However, we identified hundreds to thousands of genes and
458 pathways that oscillate in MYC-OFF cells, and thousands of genes and pathways that were up- or down-
459 regulated by MYC when MYC is activated (MYC-ON). For those researchers who wish to probe a specific
460 gene or pathway of interest that was not listed in our top hits, complete tables will be made available online
461 at FigShare prior to full publication.

462 Our findings have implications for potential applications of chronotherapy in the treatment of cancer.
463 Chronotherapy is defined as timed administration of a drug or treatment based on circadian information, to
464 maximize efficacy and / or minimize toxicity [93]. Given that the majority of drug targets are likely to be
465 circadian [4], chronotherapy has much promise in cancer biology in particular. However, the question of
466 approach remains: should a chronotherapy strategy be designed to target the tumor at a particular time
467 when it would be most vulnerable, or instead designed to minimize toxicity? These two approaches may
468 be mutually exclusive. Our findings suggest that circadian phenotype of the tumor matters in this question.
469 For those tumors with MYC amplification, drug targets related to metabolism and biosynthesis may lose
470 rhythmicity, which would favor a chronotherapy approach designed to reduce toxicity. Indeed, the Authors
471 of the CYCLOPS study noted that since GLUT2 is only weakly rhythmic in HCC, a cancer often driven by
472 MYC, use of the GLUT2-targeting streptozocin should be timed to minimize dose-limiting toxicity in the liver
473 and kidney [21]. In contrast, a separate study focusing on molecular clock gene expression in cancer
474 found that many clinically actionably genes, including those related to metabolism, correlated with clock
475 gene expression across cancer types [20]. This suggests that in cancers that retain rhythmicity (such as
476 those driven by RAS mutations), a chronotherapy approach might instead focus on timing treatment for
477 maximum efficacy against targets in the cancer cells themselves. Overall, our findings suggest that MYC
478 amplification, with further study, might emerge as a prognostic indicator for circadian function which could
479 guide chronotherapy treatment options in the future.
480

Limitations of Study:

Several limitations of this study are noted. Cancer cells are continuously proliferating, and MYC did not further enhance proliferative capacity of any of the 3 cell lines. This makes deconvoluting circadian rhythms and cell cycle oscillations challenging. While we did note that some cell cycle genes and pathways shift to oscillatory expression when MYC was expressed (**Table 1, Supplemental Figure 2**), a system where MYC induces proliferation of quiescent cells would be better suited to determine how MYC induces cell cycle rhythmicity. All studies were performed *in vitro* in cell culture conditions. While these conditions are ideal to determine free-running and cell-autonomous oscillations, particularly of metabolites [10, 58, 60], it remains to be determined which oscillatory genes and metabolites MYC disrupts *in vivo*. Finally, we noted that many genes and metabolites gained oscillation when MYC was activated, but did not probe the mechanism of these oscillations (**Supplemental Figure 1,2,6,7**). Since BMAL1 is suppressed but not eliminated by MYC, it is conceivable that these oscillations arise from residual activity of the molecular clock, blocked from its normal activity by elevated MYC levels. Alternately, these oscillations may arise from active cell cycling or in response to gain in oscillation of specific metabolites with MYC-ON (**Supplemental Figure 7**).

Methods and materials

Cell culture and circadian entrainment

U2OS MYC-ER, SHEP N-MYC-ER, and SKNAS N-MYC-ER were described previously [31, 94, 95]. Cells were cultured in DMEM high glucose (Gibco and Corning) with penicillin-streptomycin (Gibco) and 10% FBS (Hyclone). U2OS MYC-ER cells were cultured with 100 µg/mL Zeocin (Thermo Scientific) except during experiments, to maintain MYC-ER expression. For circadian time-series experiments, cells were plated at 100,000 cells / mL. 24 hours later, cells were treated with ethanol or 0.5 µM 4-hydroxytamoxifen (4OHT) to activate MYC-ER or N-MYC-ER. 24 hours later, cells were treated with 0.1 µM dexamethasone (Sigma) to entrain the molecular circadian clock. 24 hours after dexamethasone treatment, cells were detached from the plate with trypsin EDTA 0.25% (Gibco) and were collected for RNA in the following intervals: U2OS replicate 1: every 4 hours for 48 hours; U2OS replicate 2: every 2 hours for 48 hours;

SHEP replicates 1 and 2: every 4 hours for 52 hours; SKNAS: every 4 hours for 52 hours for MYC-OFF, 48 hours for MYC-ON.

RNA collection and qPCR

Cells were lysed and RNA was isolated using the RNEasy Plus mini kit (Qiagen). RNA was reverse transcribed to cDNA using the ABI Reverse Transcription Reagents system, using oligo dT for priming (Thermo Scientific). qPCR was performed with cDNA using Power Sybr Green Master Mix (Thermo Scientific) and with the Viia7 quantitative PCR machine (Applied Biosystems). Triplicate technical replicates were performed, outlier replicates (defined as being more than 1 Ct away from other two replicates) were discarded, and relative mRNA was assessed by the ΔΔCt, scaled to the first MYC-OFF timepoint and normalized to *β2M* (β2 microglobulin). Error bars are standard error of the mean (S.E.M.) of the two biological replicates described above. For U2OS, only the 4-hour resolution timepoints were used for Replicate 2.

Table of primer sequences used

Target	Primer sequences (Forward, Reverse)	Source
PER2	GGATGCCCGCCAGAGTCCAGAT, TGTCCACTTTCGAAGACTGGTCGC	[31]
NR1D1 (REV-ERBα)	TGGACTCCAACAACAACACAG, GATGGTGGGAAGTAGGTGGG	[31]
B2M	GGCCGAGATGTCTCGCTCCG, TGGAGTACGCTGGATAGCCTCC	[31]

Protein collection, immunoblot, and glycosylation detection

U2OS MYC-ER, SHEP N-MYC-ER, and SKNAS N-MYC-ER were plated at 100,000 cells / mL. 24 hours later, cells were treated with ethanol or 4-hydroxytamoxifen to activate MYC-ER or N-MYC-ER. 24 hours later, cells were treated with 0.1 μM dexamethasone (Sigma) to entrain the molecular circadian

clock. 24 hours after dexamethasone treatment, cells were detached from the plate with trypsin EDTA 0.25% (Gibco) and were collected every 2-4 hours for up to 48 hours. Protein was lysed using the M-Per lysis reagent (Thermo Scientific) with protease inhibitor cocktail (Promega) and phosphatase inhibitors 2 and 3 (Sigma). Lysates incubated on ice for at least 20 minutes, then centrifuged at > 13,000 xg, and supernatant was collected. Protein was quantified using the Bio-Rad DC Protein Assay Kit (Bio-Rad), and lysates of equal concentration were prepared for immunoblot. To detect glycosylated protein, protein samples were prepared with sample buffer that contains 10% glycerol (Sigma) and 5% 2-mercaptoethanol (Sigma), and incubated at room temperature instead of boiled, as previously described [66]. 20 µg of each sample was prepared and run by SDS-PAGE on Bio-Rad Criterion 4-15% 26-well gradient gel (Bio-Rad). For some samples (U2OS CT26, SHEP CT32, SKNAS CT 32), 20 µg was treated with PNGase-F to remove glycosylation marks, according to manufacturer's instructions (New England Biolabs). For these samples, only 12 µg of protein lysate was loaded onto the Criterion gel. Gels were transferred using the iBlot2 semi-dry blotting system to nitrocellulose membranes (Thermo Scientific). The following primary antibodies were used: rabbit anti-4F2hc/CD98 D6O3P mAb (Cell Signaling 13180), rabbit anti-LAT1 (Cell Signaling 5347), rabbit anti-GLUT1 EPR3915 mAb (Abcam ab115730), rabbit anti-REV-ERBα E1Y6D mAb (Cell Signaling 13418), rabbit anti-BMAL1 D2L7G mAb (Cell Signaling 14020) and mouse anti-α-Tubulin DM1A mAb (EMD Millipore CP06-100UG). The following secondary antibodies were used: goat anti-rabbit Alexa Flour 680 (Thermo Scientific A21109) and goat anti-mouse Alexa Flour 790 (Thermo Scientific A11357). Membranes were digitally imaged using a Licor Odyssey CLx infrared imager (Licor). U2OS data represent two independent experiments, and one experiment each for SHEP and SKNAS.

On-cell western

On-cell western [68] was performed with U2OS MYC-ER cells. 72,000 cells were plated in each well of a 24-well plate, and 24 hours later, treated ± 4OHT for 48 hours. Cells were then fixed with 3.7% paraformaldehyde (Sigma) but not permeabilized. Wells were washed with tris-buffered saline, and stained with primary antibodies mouse anti-LAT1 BU53 (Novus NBP2-50465AF647) or mouse IgG2A isotype control (Novus IC003R), and secondary antibodies goat anti-mouse Alexa Flour 790 (Thermo Scientific

A11357) or CellTag 700 Stain (Licor 926-41090), which is used to quantify total cell number and intensity. The stained plate was then digitally imaged using a Licor Odyssey CLx infrared imager (Licor), and well intensities in both channels (700 nM for CellTag, 800 for LAT1 or isotype control) were quantified using ImageStudio software (Licor). Individual wells were treated as biological replicates, and results are representative of two separate experiments.

RNA sequencing

RNA-sequencing was performed either at the University of Pennsylvania Genomic and Sequencing Core (U2OS) or by Novogene (SHEP and SKNAS). For U2OS, we activated MYC-ER in cells for 24 hours with 4-hydroxytamoxifen (4OHT, MYC-ON), or used vehicle control (MYC-OFF). We then entrained cells circadian rhythms with dexamethasone. 24 hours after dexamethasone treatment, cells were then collected every 4 hours (replicate 1) or 2 hours (replicate 2) for up to 48 hours, and RNA was extracted. CT refers to circadian time, ie, hours after dexamethasone entrainment. RNA at approximately 100 ng/µL was submitted to the University of Pennsylvania Next Generation Sequencing Core, was analyzed by BioAnalyzer and determined to have an average RNA Integrity Number (RIN) of 9.9. RNA-sequencing was performed on ribosome-depleted total RNA (replicate 1) or polyadenylated mRNAs (replicate 2) as 100 base single-end sequencing using an Illumina HiSeq 4000, yielding an average of 74.3 million reads per sample for replicate 1, and 40.9 million reads per sample for replicate 2. For SHEP and SKNAS, we activated N-MYC-ER in cells for 24 hours with 4-hydroxytamoxifen (4OHT, MYC-ON), or used vehicle control (MYC-OFF). We then entrained cells circadian rhythms with dexamethasone. 24 hours after dexamethasone treatment, cells were then collected every 4 hours for up to 52 hours, and RNA was extracted. RNA at approximately 37 ng/µL was submitted to Novogene Co., was analyzed by BioAnalyzer and determined to have an average RNA Integrity Number (RIN) of 9.8. RNA-sequencing was performed on polyadenylated mRNAs using an Illumina NovaSeq 6000 as 150 base paired end sequencing, yielding an average of 54.7 million reads per sample (when adding together both paired ends). For all RNA-sequencing output, reads were mapped with Salmon, and collapsed to gene level with Tximport. Two

biological replicate time-series experiments were performed in SHEP, and a single time-series was performed in SKNAS.

Processing of raw RNA-sequencing data

Raw reads were processed by Novogene to demultiplex, remove reads containing adaptors, remove reads containing N > 10% (N represents the base cannot be determined), and remove reads containing low quality (Qscore<= 5) base which is over 50% of the total base. Raw reads were processed by the University of Pennsylvania Next Generation Sequencing Core to demultiplex using bcl2fastq2-v2.17.1.14. All processed reads were mapped to transcripts using Salmon 1.3.0 [96] in mapping-based mode for paired-end samples, using a decoy-aware transcriptome built from Gencode v35 GRCh38 primary assembly genome and v35 transcriptome. Transcripts were collapsed to gene-level using Tximport 1.12.3 [97] using Gencode v35 transcriptome. Genes were annotated with symbols using the Ensembl GRCh38.101 transcriptome annotations. Tximport yielded as outputs raw counts, which were used for differential expression analysis, and read and length-normalized TPM (Transcripts per million), which were used for ECHO circadian rhythm analysis.

Metabolite collection and mass-spectrometry

U2OS MYC-ER were plated at 100,000 cells / mL. 24 hours later, cells were treated with ethanol or 4-hydroxytamoxifen to activate MYC-ER or N-MYC-ER. 24 hours later, cells were treated with 0.1 μM dexamethasone (Sigma) to entrain the molecular circadian clock. 24 hours after dexamethasone treatment, cells were gently scraped from the plate in ice-cold PBS (Gibco), pelleted, and snap frozen. Polar metabolites were extracted with methanol and chloroform and redissolved after drying into an acetonitrile:water mixture using a modified Bligh-Dyer method, as previously described [10, 98, 99]. Solubilized polar metabolites were subject to ultraperformance liquid chromatography (UPLC) on a Waters Acquity UPLC coupled to a Waters TQD mass spectrometer (Waters Corporation) as previously described [10, 100].

Following UPLC, mass spectrometry was performed on a QQQ quadrupole instrumentation, (Xevo TQD or TQS-micro, Waters Corporation), as previously described [10, 100]. Specific metabolites were tarted with multiple reaction monitoring, validated against standards and / or mass-spectrometry databases. Note that the panel of standards was heavily altered between when Replicate A and Replicate B were run; hence, these experiments are presented as individual replicates rather than being averaged. Each sample acquired multiple times, and the sample queue was randomized to remove bias [101]. For each Replicate, the entire set of injections was bracketed by standard metabolites at both the beginning and the end of the run to evaluate instrument performance, sensitivity, and reproducibility.

Mass spectrometry output data were processed as previously described [10], using Waters TargetLynx software (version 4.1), with ion counts processed in R using a custom script. To account for instrument drift, quality control samples, which were a pool of all samples, were injected at the start of every batch for UPLC column equilibration and every 6 injections during mass spectrometry analysis. To normalize each metabolic feature, a LOESS function (locally-weighted scatterplot smoothing) was fitted to the QC data. These values were used for ECHO analysis of circadian rhythmicity. Amino acid quantitation presented in **Figure 5F** and **Supplemental Figure 5** were further normalized to cell counts, which were taken every six hours during the time-series described above. Missing cell counts were interpolated from neighboring values. Metabolite data will be made available at Metabolomics Workbench prior to full publication.

Circadian analysis with ECHO, and graphing of circadian data in the R programming language

The Extended Circadian Harmonic Oscillator (ECHO) application [37] was chosen for oscillation analysis of RNA-sequencing and metabolomics data because it uses parametric approaches to determine rhythmicity in dampening oscillators, which are commonly observed in cell lines. ECHO v4.0 was used with the following parameters: paired replicates (where applicable), unexpressed genes or metabolites removed, linear trends removed, and default parameters for determined if a gene or metabolite is harmonic, overexpressed, or repressed. Genes or metabolites were determined to have circadian rhythmicity if they had a period between 20-28 hours, a BH.Adj.P < 0.05, and were not overexpressed or

repressed (ie, sharply increasing or decreasing over the time series by more than an amplitude change coefficient of 0.15). For heatmap data in **Figures 1 and 6** and **Supplementary Figures 1 and 6**, data were scaled using the Rescale R package to between -2 and 2 for each gene or metabolite, so they could be compared to each other, and then were sorted by phase ('hours.shifted'). Gene level data are graphed as heatmaps in ggplot2 using the civvidis colorblind-compliant color scale, and are presented as detrended TPM values ('original'), while metabolites are presented as computed cosine fit ('smoothed'), as previously performed [31]. For amplitude analysis in **Supplemental Figure 1C**, amplitudes ('initial.amplitude') of significant oscillators as defined above were plotted with ggplot2 using a mirrored histogram and logarithmic scale. Dot and line plots in **Figure 6** and **Supplemental Figures 2 and 6**, dots represent detrended TPM values or normalized abundance metabolite values, and lines represent computed cosine fit, as previously performed [31].

Differential expression with DeSeq2

Differential expression of counts data from MYC-ON vs MYC-OFF was performed using DeSeq2 v1.24.0 [48]. For each cell line, every timepoint from each replicate, where applicable, was used as a biological replicate for MYC-OFF and MYC-ON. The DeSeq2 design included time and condition, the alpha cutoff for significant enrichment was set at 0.05, and the apeglm algorithm [102] was used to normalize and shrink the results ('lfcshrink'). Genes with a padj ≤ 0.05 log 2 fold change between MYC-ON vs MYC-OFF were determined to be significant and used for further analysis.

Pathway enrichment workflow: Gene Set Enrichment Analysis (GSEA)

Gene Set Enrichment Analysis (GSEA) was performed using GSEA software v4.0 and the Molecular Signatures Database Human Genesets v7 [51-54]. Genes with a log 2 fold change ≥ ± 0.15, representing a 10% or greater change, and a padj ≤ 0.05, were subsetted for GSEA PreRanked, using default parameters. The 10% or greater change cutoff was used because GSEA tests potentially small changes across entire pathways, which may not be represented if only large gene expression changes are included [51-54]. Gene sets with less than 15 genes or more than 500 genes were excluded. GSEA

results with an FDR q-value ≤ 0.25 were determined to be significant, as was previously described [51]. Results from molecular signature databases that were not available for Phase Set Enrichment Analysis (below) and for micro RNAs were excluded from analysis for purposes of this manuscript, but full results will be made available online at FigShare prior to full publication. GSEA results are presented as normalized enrichment score (NES).

Pathway enrichment workflow: Phase Set Enrichment Analysis (PSEA)

Phase Set Enrichment Analysis (PSEA) was used to determine which pathways were enriched for genes that oscillated with a similar phase [40]. For each ECHO analysis (MYC-OFF and MYC-ON for SHEP, SKNAS, and U2OS), phases ('hours.shifted') from genes determined to have significant circadian oscillation were used along with gene names for PSEA analysis. PSEA v1.1 was run using default parameters, querying for oscillations up to 28 hours, and using the following Molecular Signatures Databases (all v7): C2 (curated gene sets), C3 (regulatory target gene sets), C5 (ontology gene sets), C6 (oncogenic signature gene sets), C7 (immunologic signature gene sets), and H (hallmark gene sets). Gene sets with a Kuiper q-value (vs. background) < 0.2 and p-value (vs. background) <0.1 were determined to be significant. As with GSEA, micro RNA-related results were excluded from analysis for purposes of this manuscript, but full results will be made available online at FigShare prior to full publication. For plotting on a polar histogram, results were binned by phase (rounded to the nearest whole number), and plotted on a 28-hour histogram using ggplot2. For bar charts, -LogP was computed from the p value of significantly enriched sets, and plotted. For instances where the p value was equal to 0, the –log p value was arbitrarily set to be less than 1 unit higher than the next most significant value in the set.

Pathway enrichment workflow: ToppFun

ToppFun functional enrichment [43] was used as an alternate method for pathway enrichment of circadian oscillating genes, and genes regulated by MYC. For circadian oscillating genes, all genes that were determined to be significantly rhythmic in each cell line in MYC-OFF or MYC-ON conditions (see "Circadian analysis with ECHO", above) were entered into ToppFun. For genes regulated by MYC,

DeSeq2 for MYC-ON vs MYC-OFF was subsetted for genes with a log 2 fold change ≥ ± 0.66, representing a 1.5-fold or greater change, and a padj ≤ 0.05. In all cases, the default background set for each category was used. When an inputted gene was not found, the default suggested alternative was used. Gene sets were limited to between 5 and 500 genes. An FDR.Q of ≤ 0.05 was considered to be significant. For this manuscript, only GO and Pathway analyses were considered and graphed, but full results will be made available online at FigShare prior to full publication. For bar charts, -LogP was computed from the p value of significantly enriched sets, and plotted. For instances where the p value was equal to 0, the –log p value was arbitrarily set to be less than 1 unit higher than the next most significant value in the set.

Pathway enrichment workflow: MetaboAnalyst Enrichment Analysis

MetaboAnalyst enrichment analysis [103] was used to determine enriched pathways among circadian metabolites. Metabolites determined to be circadian in MYC-OFF or MYC-ON conditions (see "Circadian analysis with ECHO", above) were manually curated by peak phase, as determined by heatmap analysis, into different groups (CT10 and CT20 for MYC-OFF for both Replicates, CT4 and CT16 for MYC-ON Replicate 1, and CT0, CT8, and CT12 for MYC-ON Replicate 2). For each group, KEGG IDs [104] were inputted and compared against default background. Where multiple KEGG IDs existed for a single mass spectrometry peak, the first KEGG ID was used. Metabolites were compared against the KEGG Metabolite set library. Only results with two or more enriched metabolites were used. p ≤ 0.05 was used to determine significance, and – log p is graphed as bar charts. For plotting on a polar histogram, results were binned by phase, and plotted on a 28-hour histogram using ggplot2.

Statistical analysis

Statistical analysis and tests for significance for ECHO, GSEA, PSEA, DeSeq2, ToppFun, and MetaboAnalyst Enrichment Analysis are described above. For statistical analysis of On-cell western and mass spectrometry quantitation of amino acids, we used Welch's corrected Student's t-test ('Welch's t-test', which does not assume equal variance of sample data), with p ≤ 0.05 determined to be significant and marked with an *.

Data and code availability

RNA-sequencing data have been uploaded to NCBI GEO and are available at GEO SuperSeries GSE221174, which contains GSE221103 (SHEP and SKNAS) and GSE221173 (U2OS). Metabolite data will be made available at Metabolomics Workbench prior to full publication. All other analyses and code will be made available on Figshare prior to full publication.

Statement on colorblind compliance

All color schemes have been specifically chosen to be easily distinguishable by those with any variety of colorblindness. Colors for graphs and Venn diagrams were chosen using Colorblind Universal Design (https://jfly.uni-koeln.de/color/, acknowledgements to Dr. Masataka Okabe of the Jikei Medial School, Japan, and Dr. Kei Ito of the University of Tokyo, Institute for Molecular and Cellular Biosciences, Japan). Heat maps in R were generated using the Cividis color scale, which is adapted to colorblindness [105].

Acknowledgements

We would like to acknowledge Hannah De los Santos and Dr. Jennifer Hurley (Rensselaer Polytechnic Institute) for assistance with implementing the ECHO algorithm, Dr. Aimee Edinger (University of California Irvine) for helpful discussion on nutrient transporters, Dr. Lin Zhang (University of Pennsylvania Perelman School of Medicine) for helpful discussion on analysis of RNA-sequencing data, and Dr. Fabio Hecht Castro Medeiros (University of Rochester Medical Center) for assistance on design and creation of a graphical abstract. We would also like to acknowledge the University of Rochester Wilmot Cancer Institute Genomics Research Center for guidance on processing and analyzing RNA-sequencing data and implementing differential expression analysis. This work was supported by F30CA200347 and T32CA009140 (to ZEW), F31CA232551 (to RB), R21CA213234 and R01DK120757 (to AMW), R01CA057431 and R01CA051497 (to CVD), and R00CA204593 (to BJA). SSM and BJA were also supported by the Wilmot Cancer Institute.

Author Contributions

Conceptualization: J.C., A.M.W., C.V.D., and B.J.A.; **Methodology**: R.E.D., A.L.H., A.M.W., and B.J.A.; **Software**: R.E.D., S.K., J.B.B., D.M., R.B., S.S.M., A.M.W., and B.J.A.; **Validation**: R.E.D., J.C., S.K., A.M.W., and B.J.A.; **Formal analysis**: R.E.D., J.C., J.B.B., A.L.H., R.B., and B.J.A.; **Investigation**: R.E.D., S.N.A.B.A.S., J.B.B., D.M., S.K., A.L.H., Z.E.W., R.B., and B.J.A.; **Resources**: A.M.W., C.V.D., and B.J.A.; **Data Curation**: D.M., S.K., A.M.W., and B.J.A.; **Writing - Original Draft**: J.C. and B.J.A.; **Writing - Review & Editing**: J.C., J.B.B., Z.E.W., R.B., S.S.M., A.M.W., C.V.D., and B.J.A.; **Visualization**: R.E.D., J.C., J.B.B., S.K., R.B., and B.J.A.; **Supervision**: A.M.W., C.V.D., and B.J.A.; **Project administration**: R.E.D., A.M.W., C.V.D., and B.J.A.; **Funding acquisition**: Z.E.W., R.B., A.M.W., C.V.D., and B.J.A.

Conflict of interest

The authors declare no conflict of interest.

Figure Legends

Figure 1. Oncogenic MYC disrupts global transcriptomic circadian oscillation in cancer cells. A. SHEP N-MYC-ER and U2OS MYC-ER were treated with ethanol control (MYC-OFF) or 4-hydroxytamoxifen (MYC-ON) (4OHT) to activate MYC, and entrained with dexamethasone, and after 24 hours, RNA was collected every 2-4 hours for the indicated time period. Expression of the indicated genes was determined by quantitative PCR (qPCR), normalized to β2M. CT = circadian time. Note the inset MYC-OFF only graph for SHEP *NR1D1*, to show oscillation of *NR1D1* in MYC-OFF cells on a different scale. **B.** RNA-sequencing was performed on SHEP N-MYC-ER, SKNAS-N-MYC-ER or U2OS MYC-ER ± 4OHT and + dexamethasone, with RNA samples collected every 2-4 hours at the indicated timepoints. RNA was analyzed for rhythmicity by ECHO for both MYC-OFF and MYC-ON, with genes with a 20-28 hour period and with BH.Adj.P.Value < 0.05 deemed rhythmic. These genes were sorted by phase and are presented in a heatmap for MYC-OFF. For MYC-ON, the same genes that are rhythmic in MYC-OFF are presented in the same order, but with MYC-ON values instead.

Figure 2. Oncogenic MYC shifts the identify of oscillating transcriptional programs. A. Oscillatory genes in SHEP N-MYC-ER, SKNAS-N-MYC-ER or U2OS MYC-ER were analyzed with Phase Set Enrichment Analysis (PSEA) for oscillatory pathway enrichment, with a period of 20 – 28 hours and q-value (vs. background)` < 0.2 and p-value (vs. background) <0.1 deemed significant. Oscillatory pathways were binned by hour and plotted on a polar histogram, which is a circular histogram that accurately displays a repeating circadian scale on the X-axis. The Y-axis scale for each histogram is on the left side. MYC-OFF significant pathways are shown, and the same pathways are also plotted for MYC-ON. **B.** Overlap of oscillatory programs in MYC-OFF are shown by Venn diagram, and identity of oscillatory programs are plotted by average of –LogP from each cell line of overlap. The most highly significant pathways (up to 10) for each overlap are shown.

Figure 3. MYC upregulates biosynthetic and metabolic processes and suppresses cell adhesion processes across cancer cell lines. A. Differential expression analysis, using DeSeq2, was performed on MYC-ON vs MYC-OFF for SHEP N-MYC-ER, SKNAS-N-MYC-ER or U2OS MYC-ER, with p.adj < 0.05 deemed significant. Genes that were up- or down-regulated in MYC-ON by at least 10% are shown. **B,C.** Gene Set Enrichment Analysis (GSEA) was performed on genes up- or down-regulated by at least 10% in each cell line using GSEA Pre-Ranked, with gene sets with FDR q-val < 0.25 deemed significant. Venn diagrams of overlapping gene sets from MYC-ON upregulated (**B**) and MYC-ON downregulated processes (**C**) are shown, and the most highly significant pathways (up to 10) for each overlap are shown, ranked by Normalized Enrichment Score. For all graphed pathways, FDR.q < 0.002.

Figure 4. Oncogenic MYC shifts oscillatory gene expression to static non-oscillatory regulation. A. Illustration of workflow to identify pathways that lose oscillation when MYC is activated (by PSEA), and which of these pathways become up- or down-regulated by MYC (using GSEA). **B, C**. Venn diagram from SHEP N-N-MYC-ER (**B**) and SKNAS N-MYC-ER (**C**) of pathways (identified by PSEA) that were circadian in MYC-OFF (center, green), and lost oscillation and became either downregulated (left, pink) or

upregulated (right, tan) in MYC-ON (identified by GSEA). **D,E.** The most highly significant downregulated and upregulated pathways that lost oscillation from SHEP (**B**) and SKNAS (**C**) are shown, as ranked by Normalized Enrichment Score from GSEA. FDR.q for graphed pathways = 0 for SHEP and SKNAS oscillating to MYC-upregulated, FDR.q < 0.051 for SKNAS oscillating to MYC-downregulated.

Figure 5. Rhythmic glycosylation and expression of nutrient transporters are disrupted by MYC. A-C. U2OS MYC-ER (**A**), SHEP N-MYC-ER, (**B**), and SKNAS N-MYC-ER (**C**) were treated with ethanol control (MYC-OFF) or 4- hydroxytamoxifen (MYC-ON) (4OHT) to activate MYC, and entrained with dexamethasone, and after 24 hours, protein was collected every 4 hours for the indicated time period. Protein lysates were prepared to preserve protein glycosylation (see Methods), and immunoblot was performed for the indicated proteins. For some targets [4F2hc, LAT1, REV-ERBα (abbreviated REVα)], a darker exposure ('dark') and lighter exposure ('light') of the same blot are presented. For GLUT1, # indicates a non-specific band. Some samples (CT26 for U2OS, CT32 for SHEP and SKNAS) were treated with PNGase-F prior to immunoblot to remove glycosylation marks. Note that the PNGase-F lanes have less protein loaded than the other lanes. Data represent n=2 biological replicates for U2OS and one each for SHEP and SKNAS. **D.** On-cell western of U2OS MYC-ER cells ± MYC for LAT1. U2OS MYC-ER cells were grown on a 24-well tissue culture plate ± 4OHT for 48 hours, fixed with formaldehyde but not permeabilized, and then stained with the indicated antibody or IgG control. CellStain 700 indicates cell density in each well. Data represent at least two independent experiments of 6 biological replicate wells each. **E.** Quantitation of LAT1 or IgG from (**D**). * indicates P < 0.00001 by Welch's Corrected Student's T-test. **F.** LC-Mass spectrometry was performed on U2OS MYC-ER treated ± 4OHT for at least 48 hours. N=25 circadian timepoints for MYC-OFF and MYC-ON were averaged as biological replicates, normalized to cell number for each collection. * indicates p < 0.05 by Welch's Corrected Student's T-test.

Figure 6. MYC disrupts metabolic circadian oscillations in a cell-autonomous manner. U2OS MYC-ER were treated with ethanol control (MYC-OFF) or 4- hydroxytamoxifen (MYC-ON) (4OHT) to activate MYC for 24 hours, and entrained with dexamethasone, and after 24 hours, cells were extracted for polar

metabolites every 2 hours for the indicated time period. Mass spectrometry was performed, and rhythmicity was assessed by ECHO for both MYC-OFF and MYC-ON, with metabolites with a 20-28 hour period and with BH.Adj.P.Value < 0.05 deemed rhythmic. These metabolites were sorted by phase and are presented in a heatmap for MYC-OFF. For MYC-ON, the same metabolites that are rhythmic in MYC-OFF are presented in the same order, but with MYC-ON values instead. **B.** Metabolites deemed to be oscillating by ECHO for MYC-OFF are graphed, with dots representing the relative abundance values, and lines indicating the fitted oscillation curves as calculated by ECHO. Metabolites with a green border are oscillatory in both MYC-OFF and MYC-ON. **C.** KEGG enrichment analysis was performed on metabolites that peaked in the indicated phases in MYC-OFF or MYC-ON conditions, and significantly enriched pathways were graphed on a polar histogram. For each histogram, the scale is on the left side. Pathways with a $p < 0.05$ were deemed significant and are graphed.

Figure 7 / Graphical Abstract.

Supplemental Figures and Tables

Supplemental Figure 1. Overlap of oscillating genes in MYC-OFF cells, and impact of MYC on gain of oscillation. A. The overlap of oscillating genes identified in **Figure 1A** is shown by Venn diagram. **B.** RNA-sequencing was performed on SHEP N-MYC-ER, SKNAS-N-MYC-ER or U2OS MYC-ER ± 4OHT and + dexamethasone, with RNA samples collected every 2-4 hours at the indicated timepoints. RNA was analyzed for rhythmicity by ECHO for both MYC-OFF and MYC-ON, with genes with a 20-28 hour period and with BH.Adj.P.Value < 0.05 deemed to be rhythmic. These genes were sorted by phase and are presented in a heatmap for MYC-ON. For MYC-OFF, the same genes that are rhythmic in MYC-OFF are presented in the same order, but with MYC-OFF values instead. N=2 time series were used for SHEP and U2OS, N=1 time series was used for SKNAS. **C.** The amplitude of oscillation of each gene in MYC-OFF and MYC-ON, as determined by ECHO, was graphed as a mirrored density plot to allow direct comparison between each condition, with MYC-OFF on the top and MYC-ON on the bottom.

Supplemental Figure 2. MYC induces an alternate oscillatory program that includes cell cycle. A. The pathways deemed to be significantly oscillatory in MYC-ON cells by PSEA (20-28 hr period, q-value (vs. background) < 0.2 and p-value (vs. background) <0.1) for each cell line were binned and graphed on a polar histogram. The scale for each histogram is on the left side. Overlap of oscillatory programs by Venn diagram is also shown. **B.** The identity of oscillatory programs in MYC-ON cells from (**A**) are plotted by average of –LogP from each cell line of overlap. The most highly significant pathways (up to 10) for each overlap are shown. **C,D.** Cell cycle genes deemed to be oscillating by ECHO for MYC-OFF and MYC-ON SHEP (**D**) and U2OS (**E**) are graphed, with dots representing the RNA-sequencing TPM values, and lines indicating the fitted oscillation curves as calculated by ECHO. Genes with a green border are oscillatory in both MYC-OFF and MYC-ON.

Table 1. An independent methodology reveals oscillating gene pathways in MYC-inducible cells. Genes from SHEP N-MYC-ER, SKNAS-N-MYC-ER or U2OS MYC-ER MYC-OFF or MYC-ON that were deemed oscillatory by ECHO, without regards to their phase, were analyzed for pathway enrichment with the ToppFun suite, and pathways with FDR B&H < 0.05 were deemed significant. The most highly enriched pathways from the Pathway and GO libraries are shown in the table, ranked by –LogP.

Supplemental Figure 3. The most altered genes by MYC correlate with changes in biosynthesis, metabolism, and cell attachment. A. Differential expression analysis, using DeSeq2, was performed on MYC-ON vs MYC-OFF for SHEP N-MYC-ER, SKNAS-N-MYC-ER or U2OS MYC-ER, with p.adj < 0.05 deemed significant. Genes that were up- or down-regulated in MYC-ON by at least 1.5-fold are shown. **B,C.** Venn diagram of the overlap of 1.5-fold upregulated (**B**) and downregulated (**C**) genes by MYC. **D, E.** Genes that were upregulated or downregulated in all 3 cell lines were subjected to pathway analysis with the ToppFun suite, and pathways with FDR B&H < 0.05 were deemed significant. For upregulated (**D**) and downregulated (**E**) genes, the most highly enriched pathways from the Pathway and GO libraries are shown in the table, ranked by –LogP.

Supplemental Figure 4. A gene-centric methodology reveals pathways that shift from oscillatory to MYC-regulated. A. Illustration of workflow to identify genes that lose oscillation when MYC is activated (by ECHO), which of these genes become up- or down-regulated by MYC (using DeSeq2), and analysis of these genes for pathway enrichment by ToppFun. **B-D.** Venn diagram from SHEP N-N-MYC-ER (**B**), SKNAS N-MYC-ER (**C**), or U2OS MYC-ER (**D**) of genes (identified by ECHO) that were circadian in MYC-OFF (center, green), and lost oscillation and became either downregulated (left, pink) or upregulated (right, tan) in MYC-ON (identified by DeSeq2). Bottom section shows the most highly enriched upregulated pathways in each cell line, as identified by ToppFun enrichment from the Pathway and GO libraries of genes that lost oscillation and became upregulated. Pathways are ranked by –LogP, and FDR B&H < 0.05 for all pathways.

Supplemental Figure 5. MYC enhances intracellular amino acid pools. A replicate experiment (Replicate B) of **Figure 5F** was performed. LC-Mass spectrometry was performed on U2OS MYC-ER treated ± 4OHT for at least 48 hours. N=25 circadian timepoints for MYC-OFF and MYC-ON were averaged as biological replicates, normalized to cell number for each collection. * indicates $p < 0.05$ by Welch's Corrected Student's T-test.

Supplemental Figure 6. MYC disrupts cell autonomous oscillations in a replicate experiment, but induces alternate oscillations. A. An independent replicate ('Replicate B') of time-series metabolite collection from U2OS MYC-ER cells was performed in an identical fashion to that described in **Figure 6A**. Rhythmicity was assessed by ECHO for both MYC-OFF and MYC-ON, with metabolites with a 20-28 hour period and with BH.Adj.P.Value < 0.05 deemed rhythmic. These metabolites were sorted by phase and are presented in a heatmap for MYC-OFF. For MYC-ON, the same metabolites that are rhythmic in MYC-OFF are presented in the same order, but with MYC-ON values instead. **B.** Metabolites from Replicate B deemed to be oscillating by ECHO for MYC-OFF are graphed, with dots representing the relative abundance values, and lines indicating the fitted oscillation curves as calculated by ECHO. Metabolites with a green border are oscillatory in both MYC-OFF and MYC-ON. **C, D. For Replicate A** (**C**) from

Figure 6, and **Replicate B** (**D**), metabolites deemed oscillatory from MYC-ON are shown, sorted by phase. For MYC-OFF, the same metabolites that are rhythmic in MYC-ON are presented, but with MYC-OFF values instead.

Supplemental Figure 7. MYC disrupts metabolic circadian programming. A,B. KEGG enrichment analysis was performed on metabolites that peaked in the indicated phases from Replicate B in MYC-OFF (**A**) or MYC-ON (**B**) conditions, and significantly enriched pathways were graphed on a polar histogram. For each histogram, the scale is on the left side. Pathways with a $p < 0.05$ were deemed significant and are graphed.

References

1. Partch, C.L., Green, C.B., and Takahashi, J.S., *Molecular architecture of the mammalian circadian clock.* Trends in cell biology, 2014. **24**(2): p. 90-9.
2. Bugge, A., Feng, D., Everett, L.J., Briggs, E.R., Mullican, S.E., Wang, F., Jager, J., and Lazar, M.A., *Rev-erbalpha and Rev-erbbeta coordinately protect the circadian clock and normal metabolic function.* Genes Dev, 2012. **26**(7): p. 657-67.
3. Cho, H., Zhao, X., Hatori, M., Yu, R.T., Barish, G.D., Lam, M.T., Chong, L.W., DiTacchio, L., Atkins, A.R., Glass, C.K., Liddle, C., Auwerx, J., Downes, M., Panda, S., and Evans, R.M., *Regulation of circadian behaviour and metabolism by REV-ERB-alpha and REV-ERB-beta.* Nature, 2012. **485**(7396): p. 123-7.
4. Zhang, R., Lahens, N.F., Ballance, H.I., Hughes, M.E., and Hogenesch, J.B., *A circadian gene expression atlas in mammals: implications for biology and medicine.* Proc Natl Acad Sci U S A, 2014. **111**(45): p. 16219-24.
5. Mure, L.S., Le, H.D., Benegiamo, G., Chang, M.W., Rios, L., Jillani, N., Ngotho, M., Kariuki, T., Dkhissi-Benyahya, O., Cooper, H.M., and Panda, S., *Diurnal transcriptome atlas of a primate across major neural and peripheral tissues.* Science, 2018. **359**(6381).
6. Trott, A.J. and Menet, J.S., *Regulation of circadian clock transcriptional output by CLOCK:BMAL1.* PLoS Genet, 2018. **14**(1): p. e1007156.
7. Yeung, J., Mermet, J., Jouffe, C., Marquis, J., Charpagne, A., Gachon, F., and Naef, F., *Transcription factor activity rhythms and tissue-specific chromatin interactions explain circadian gene expression across organs.* Genome Res, 2018. **28**(2): p. 182-191.
8. Hurley, J.M., Jankowski, M.S., De Los Santos, H., Crowell, A.M., Fordyce, S.B., Zucker, J.D., Kumar, N., Purvine, S.O., Robinson, E.W., Shukla, A., Zink, E., Cannon, W.R., Baker, S.E., Loros, J.J., and Dunlap, J.C., *Circadian Proteomic Analysis Uncovers Mechanisms of Post-Transcriptional Regulation in Metabolic Pathways.* Cell Syst, 2018. **7**(6): p. 613-626 e5.
9. Collins, E.J., Cervantes-Silva, M.P., Timmons, G.A., O'Siorain, J.R., Curtis, A.M., and Hurley, J.M., *Post-transcriptional circadian regulation in macrophages organizes temporally distinct immunometabolic states.* Genome Res, 2021. **31**(2): p. 171-85.
10. Krishnaiah, S.Y., et al., *Clock Regulation of Metabolites Reveals Coupling between Transcription and Metabolism.* Cell Metab, 2017. **25**(4): p. 961-974 e4.
11. Kettner, N.M., Voicu, H., Finegold, M.J., Coarfa, C., Sreekumar, A., Putluri, N., Katchy, C.A., Lee, C., Moore, D.D., and Fu, L., *Circadian Homeostasis of Liver Metabolism Suppresses Hepatocarcinogenesis.* Cancer Cell, 2016. **30**(6): p. 909-924.
12. Papagiannakopoulos, T., Bauer, M.R., Davidson, S.M., Heimann, M., Subbaraj, L., Bhutkar, A., Bartlebaugh, J., Vander Heiden, M.G., and Jacks, T., *Circadian Rhythm Disruption Promotes Lung Tumorigenesis.* Cell Metab, 2016. **24**(2): p. 324-31.
13. Filipski, E., Delaunay, F., King, V.M., Wu, M.W., Claustrat, B., Grechez-Cassiau, A., Guettier, C., Hastings, M.H., and Francis, L., *Effects of chronic jet lag on tumor progression in mice.* Cancer Res, 2004. **64**(21): p. 7879-85.
14. Filipski, E., King, V.M., Li, X., Granda, T.G., Mormont, M.C., Claustrat, B., Hastings, M.H., and Levi, F., *Disruption of circadian coordination accelerates malignant growth in mice.* Pathologie-biologie, 2003. **51**(4): p. 216-9.
15. Filipski, E., Subramanian, P., Carriere, J., Guettier, C., Barbason, H., and Levi, F., *Circadian disruption accelerates liver carcinogenesis in mice.* Mutation research, 2009. **680**(1-2): p. 95-105.
16. Logan, R.W., Zhang, C., Murugan, S., O'Connell, S., Levitt, D., Rosenwasser, A.M., and Sarkar, D.K., *Chronic shift-lag alters the circadian clock of NK cells and promotes lung cancer growth in rats.* J Immunol, 2012. **188**(6): p. 2583-91.
17. Lee, Y., Lahens, N.F., Zhang, S., Bedont, J., Field, J.M., and Sehgal, A., *G1/S cell cycle regulators mediate effects of circadian dysregulation on tumor growth and provide targets for timed anticancer treatment.* PLoS Biol, 2019. **17**(4): p. e3000228.
18. Chun, S.K., Fortin, B.M., Fellows, R.C., Habowski, A.N., Verlande, A., Song, W.A., Mahieu, A.L., Lefebvre, A., Sterrenberg, J.N., Velez, L.M., Digman, M.A., Edwards, R.A., Pannunzio, N.R., Seldin, M.M., Waterman, M.L.,

and Masri, S., *Disruption of the circadian clock drives Apc loss of heterozygosity to accelerate colorectal cancer.* Sci Adv, 2022. **8**(32): p. eabo2389.

19. Stokes, K., Nunes, M., Trombley, C., Flôres, D.E.F.L., Wu, G., Taleb, Z., Alkhateeb, A., Banskota, S., Harris, C., Love, O.P., Khan, W.I., Rueda, L., Hogenesch, J.B., and Karpowicz, P., *The Circadian Clock Gene, Bmal1, Regulates Intestinal Stem Cell Signaling and Represses Tumor Initiation.* Cellular and Molecular Gastroenterology and Hepatology, 2021. **12**(5): p. 1847-1872.e0.
20. Ye, Y., Xiang, Y., Ozguc, F.M., Kim, Y., Liu, C.J., Park, P.K., Hu, Q., Diao, L., Lou, Y., Lin, C., Guo, A.Y., Zhou, B., Wang, L., Chen, Z., Takahashi, J.S., Mills, G.B., Yoo, S.H., and Han, L., *The Genomic Landscape and Pharmacogenomic Interactions of Clock Genes in Cancer Chronotherapy.* Cell Syst, 2018. **6**(3): p. 314-328 e2.
21. Anafi, R.C., Francey, L.J., Hogenesch, J.B., and Kim, J., *CYCLOPS reveals human transcriptional rhythms in health and disease.* Proc Natl Acad Sci U S A, 2017. **114**(20): p. 5312-5317.
22. Shilts, J., Chen, G., and Hughey, J.J., *Evidence for widespread dysregulation of circadian clock progression in human cancer.* PeerJ, 2018. **6**: p. e4327.
23. Wu, G., Francey, L.J., Ruben, M.D., and Hogenesch, J.B., *Normalized coefficient of variation (nCV): a method to evaluate circadian clock robustness in population scale data.* Bioinformatics, 2021. **37**(23): p. 4581-4583.
24. Lee, Y., *Roles of circadian clocks in cancer pathogenesis and treatment.* Experimental & molecular medicine, 2021. **53**(10): p. 1529-1538.
25. Burchett, J.B., Knudsen-Clark, A.M., and Altman, B.J., *MYC Ran Up the Clock: The Complex Interplay between MYC and the Molecular Circadian Clock in Cancer.* International journal of molecular sciences, 2021. **22**(14): p. 7761.
26. Savvidis, C. and Koutsilieris, M., *Circadian rhythm disruption in cancer biology.* Mol Med, 2012. **18**: p. 1249-60.
27. Schaub, F.X., Dhankani, V., Berger, A.C., Trivedi, M., Richardson, A.B., Shaw, R., Zhao, W., Zhang, X., Ventura, A., Liu, Y., Ayer, D.E., Hurlin, P.J., Cherniack, A.D., Eisenman, R.N., Bernard, B., Grandori, C., and Cancer Genome Atlas, N., *Pan-cancer Alterations of the MYC Oncogene and Its Proximal Network across the Cancer Genome Atlas.* Cell Syst, 2018. **6**(3): p. 282-300 e2.
28. Stine, Z.E., Walton, Z.E., Altman, B.J., Hsieh, A.L., and Dang, C.V., *MYC, Metabolism, and Cancer.* Cancer Discov, 2015. **5**(10): p. 1024-39.
29. Wolf, E., Lin, C.Y., Eilers, M., and Levens, D.L., *Taming of the beast: shaping Myc-dependent amplification.* Trends in cell biology, 2015. **25**(4): p. 241-8.
30. Bretones, G., Delgado, M.D., and León, J., *Myc and cell cycle control.* Biochimica et Biophysica Acta (BBA) - Gene Regulatory Mechanisms, 2015. **1849**(5): p. 506-516.
31. Altman, B.J., et al., *MYC Disrupts the Circadian Clock and Metabolism in Cancer Cells.* Cell Metab, 2015. **22**(6): p. 1009-19.
32. Altman, B.J., Hsieh, A.L., Gouw, A.M., and Dang, C.V., *Correspondence: Oncogenic MYC persistently upregulates the molecular clock component REV-ERBalpha.* Nature communications, 2017. **8**: p. 14862.
33. Shostak, A., Ruppert, B., Diernfellner, A., and Brunner, M., *Correspondence: Reply to 'Oncogenic MYC persistently upregulates the molecular clock component REV-ERBalpha'.* Nature communications, 2017. **8**: p. 14918.
34. Shostak, A., Ruppert, B., Ha, N., Bruns, P., Toprak, U.H., Project, I.M.-S., Eils, R., Schlesner, M., Diernfellner, A., and Brunner, M., *MYC/MIZ1-dependent gene repression inversely coordinates the circadian clock with cell cycle and proliferation.* Nature communications, 2016. **7**: p. 11807.
35. Repouskou, A. and Prombona, A., *c-MYC targets the central oscillator gene Per1 and is regulated by the circadian clock at the post-transcriptional level.* Biochim Biophys Acta, 2016. **1859**(4): p. 541-52.
36. Moreno-Smith, M., Milazzo, G., Tao, L., Fekry, B., Zhu, B., Mohammad, M.A., Di Giacomo, S., Borkar, R., Reddy, K.R.K., Capasso, M., Vasudevan, S.A., Sumazin, P., Hicks, J., Putluri, N., Perini, G., Eckel-Mahan, K., Burris, T.P., and Barbieri, E., *Restoration of the molecular clock is tumor suppressive in neuroblastoma.* Nature communications, 2021. **12**(1): p. 4006.
37. De Los Santos, H., Collins, E.J., Mann, C., Sagan, A.W., Jankowski, M.S., Bennett, K.P., and Hurley, J.M., *ECHO: an Application for Detection and Analysis of Oscillators Identifies Metabolic Regulation on Genome-Wide Circadian Output.* Bioinformatics, 2019.

38. Ness-Cohn, E., Allada, R., and Braun, R., *Comment on "Circadian rhythms in the absence of the clock gene Bmal1".* Science, 2021. **372**(6539): p. eabe9230.
39. Ray, S., Valekunja, U.K., Stangherlin, A., Howell, S.A., Snijders, A.P., Damodaran, G., and Reddy, A.B., *Circadian rhythms in the absence of the clock gene Bmal1.* Science, 2020. **367**(6479): p. 800-806.
40. Zhang, R., Podtelezhnikov, A.A., Hogenesch, J.B., and Anafi, R.C., *Discovering Biology in Periodic Data through Phase Set Enrichment Analysis (PSEA).* J Biol Rhythms, 2016. **31**(3): p. 244-57.
41. Relogio, A., Westermark, P.O., Wallach, T., Schellenberg, K., Kramer, A., and Herzel, H., *Tuning the mammalian circadian clock: robust synergy of two loops.* PLoS Comput Biol, 2011. **7**(12): p. e1002309.
42. Fischer, M., Schade, A.E., Branigan, T.B., Müller, G.A., and DeCaprio, J.A., *Coordinating gene expression during the cell cycle.* Trends in Biochemical Sciences, 2022. **47**(12): p. 1009-1022.
43. Chen, J., Bardes, E.E., Aronow, B.J., and Jegga, A.G., *ToppGene Suite for gene list enrichment analysis and candidate gene prioritization.* Nucleic Acids Res, 2009. **37**(Web Server issue): p. W305-11.
44. Lin, C.Y., Loven, J., Rahl, P.B., Paranal, R.M., Burge, C.B., Bradner, J.E., Lee, T.I., and Young, R.A., *Transcriptional amplification in tumor cells with elevated c-Myc.* Cell, 2012. **151**(1): p. 56-67.
45. Nie, Z., Hu, G., Wei, G., Cui, K., Yamane, A., Resch, W., Wang, R., Green, D.R., Tessarollo, L., Casellas, R., Zhao, K., and Levens, D., *c-Myc is a universal amplifier of expressed genes in lymphocytes and embryonic stem cells.* Cell, 2012. **151**(1): p. 68-79.
46. Peukert, K., Staller, P., Schneider, A., Carmichael, G., Hänel, F., and Eilers, M., *An alternative pathway for gene regulation by Myc.* The EMBO Journal, 1997. **16**(18): p. 5672-5686.
47. Murphy, D.J., Junttila, M.R., Pouyet, L., Karnezis, A., Shchors, K., Bui, D.A., Brown-Swigart, L., Johnson, L., and Evan, G.I., *Distinct thresholds govern Myc's biological output in vivo.* Cancer Cell, 2008. **14**(6): p. 447-57.
48. Love, M.I., Huber, W., and Anders, S., *Moderated estimation of fold change and dispersion for RNA-seq data with DESeq2.* Genome biology, 2014. **15**(12): p. 550.
49. Walz, S., Lorenzin, F., Morton, J., Wiese, K.E., von Eyss, B., Herold, S., Rycak, L., Dumay-Odelot, H., Karim, S., Bartkuhn, M., Roels, F., Wustefeld, T., Fischer, M., Teichmann, M., Zender, L., Wei, C.L., Sansom, O., Wolf, E., and Eilers, M., *Activation and repression by oncogenic MYC shape tumour-specific gene expression profiles.* Nature, 2014. **511**(7510): p. 483-7.
50. Sabo, A., Kress, T.R., Pelizzola, M., de Pretis, S., Gorski, M.M., Tesi, A., Morelli, M.J., Bora, P., Doni, M., Verrecchia, A., Tonelli, C., Faga, G., Bianchi, V., Ronchi, A., Low, D., Muller, H., Guccione, E., Campaner, S., and Amati, B., *Selective transcriptional regulation by Myc in cellular growth control and lymphomagenesis.* Nature, 2014. **511**(7510): p. 488-92.
51. Subramanian, A., Tamayo, P., Mootha, V.K., Mukherjee, S., Ebert, B.L., Gillette, M.A., Paulovich, A., Pomeroy, S.L., Golub, T.R., Lander, E.S., and Mesirov, J.P., *Gene set enrichment analysis: A knowledge-based approach for interpreting genome-wide expression profiles.* Proceedings of the National Academy of Sciences, 2005. **102**(43): p. 15545.
52. Mootha, V.K., et al., *PGC-1α-responsive genes involved in oxidative phosphorylation are coordinately downregulated in human diabetes.* Nature Genetics, 2003. **34**(3): p. 267-273.
53. Liberzon, A., Birger, C., Thorvaldsdóttir, H., Ghandi, M., Mesirov, Jill P., and Tamayo, P., *The Molecular Signatures Database Hallmark Gene Set Collection.* Cell Systems, 2015. **1**(6): p. 417-425.
54. Liberzon, A., Subramanian, A., Pinchback, R., Thorvaldsdóttir, H., Tamayo, P., and Mesirov, J.P., *Molecular signatures database (MSigDB) 3.0.* Bioinformatics, 2011. **27**(12): p. 1739-1740.
55. Wolfer, A. and Ramaswamy, S., *MYC and Metastasis.* Cancer Research, 2011. **71**(6): p. 2034.
56. Lee, H.Y., Cha, J., Kim, S.K., Park, J.H., Song, K.H., Kim, P., and Kim, M.-Y., *c-MYC Drives Breast Cancer Metastasis to the Brain, but Promotes Synthetic Lethality with TRAIL.* Molecular Cancer Research, 2019. **17**(2): p. 544-554.
57. Dhanasekaran, R., Baylot, V., Kim, M., Kuruvilla, S., Bellovin, D.I., Adeniji, N., Rajan Kd, A., Lai, I., Gabay, M., Tong, L., Krishnan, M., Park, J., Hu, T., Barbhuiya, M.A., Gentles, A.J., Kannan, K., Tran, P.T., and Felsher, D.W., *MYC and Twist1 cooperate to drive metastasis by eliciting crosstalk between cancer and innate immunity.* eLife, 2020. **9**: p. e50731.

58. Clark, G.T., Yu, Y., Urban, C.A., Fu, G., Wang, C., Zhang, F., Linhardt, R.J., and Hurley, J.M., *Circadian control of heparan sulfate levels times phagocytosis of amyloid beta aggregates.* PLOS Genetics, 2022. **18**(2): p. e1009994.
59. Aviram, R., Manella, G., Kopelman, N., Neufeld-Cohen, A., Zwighaft, Z., Elimelech, M., Adamovich, Y., Golik, M., Wang, C., Han, X., and Asher, G., *Lipidomics Analyses Reveal Temporal and Spatial Lipid Organization and Uncover Daily Oscillations in Intracellular Organelles.* Mol Cell, 2016. **62**(4): p. 636-48.
60. Schmitt, K., Grimm, A., Dallmann, R., Oettinghaus, B., Restelli, L.M., Witzig, M., Ishihara, N., Mihara, K., Ripperger, J.A., Albrecht, U., Frank, S., Brown, S.A., and Eckert, A., *Circadian Control of DRP1 Activity Regulates Mitochondrial Dynamics and Bioenergetics.* Cell Metabolism, 2018. **27**(3): p. 657-666.e5.
61. Vander Heiden, M.G. and DeBerardinis, R.J., *Understanding the Intersections between Metabolism and Cancer Biology.* Cell, 2017. **168**(4): p. 657-669.
62. Yanagida, O., et al., *Human L-type amino acid transporter 1 (LAT1): characterization of function and expression in tumor cell lines.* Biochim Biophys Acta, 2001. **1514**(2): p. 291-302.
63. Bhutia, Y.D., Babu, E., Ramachandran, S., and Ganapathy, V., *Amino Acid transporters in cancer and their relevance to "glutamine addiction": novel targets for the design of a new class of anticancer drugs.* Cancer Res, 2015. **75**(9): p. 1782-8.
64. Szablewski, L., *Expression of glucose transporters in cancers.* Biochimica et Biophysica Acta (BBA) - Reviews on Cancer, 2013. **1835**(2): p. 164-169.
65. Console, L., Scalise, M., Salerno, S., Scanga, R., Giudice, D., De Bartolo, L., Tonazzi, A., and Indiveri, C., *N-glycosylation is crucial for trafficking and stability of SLC3A2 (CD98).* Scientific reports, 2022. **12**(1): p. 14570.
66. Jacobs, S.R., Herman, C.E., Maciver, N.J., Wofford, J.A., Wieman, H.L., Hammen, J.J., and Rathmell, J.C., *Glucose uptake is limiting in T cell activation and requires CD28-mediated Akt-dependent and independent pathways.* J Immunol, 2008. **180**(7): p. 4476-86.
67. Osthus, R.C., Shim, H., Kim, S., Li, Q., Reddy, R., Mukherjee, M., Xu, Y., Wonsey, D., Lee, L.A., and Dang, C.V., *Deregulation of glucose transporter 1 and glycolytic gene expression by c-Myc.* J Biol Chem, 2000. **275**(29): p. 21797-800.
68. Boveia, V. and Schutz-Geschwender, A., *Quantitative Analysis of Signal Transduction with In-Cell Western Immunofluorescence Assays*, in *Detection of Blotted Proteins: Methods and Protocols*, B.T. Kurien and R.H. Scofield, Editors. 2015, Springer New York: New York, NY. p. 115-130.
69. Wu, G., Ruben, M.D., Francey, L.J., Lee, Y.Y., Anafi, R.C., and Hogenesch, J.B., *An in silico genome-wide screen for circadian clock strength in human samples.* Bioinformatics, 2022: p. btac686.
70. Shachaf, C.M., Kopelman, A.M., Arvanitis, C., Karlsson, A., Beer, S., Mandl, S., Bachmann, M.H., Borowsky, A.D., Ruebner, B., Cardiff, R.D., Yang, Q., Bishop, J.M., Contag, C.H., and Felsher, D.W., *MYC inactivation uncovers pluripotent differentiation and tumour dormancy in hepatocellular cancer.* Nature, 2004. **431**(7012): p. 1112-7.
71. Conacci-Sorrell, M., McFerrin, L., and Eisenman, R.N., *An overview of MYC and its interactome.* Cold Spring Harbor perspectives in medicine, 2014. **4**(1): p. a014357.
72. Pariollaud, M., Ibrahim, L.H., Irizarry, E., Mello, R.M., Chan, A.B., Altman, B.J., Shaw, R.J., Bollong, M.J., Wiseman, R.L., and Lamia, K.A., *Circadian disruption enhances HSF1 signaling and tumorigenesis in Kras-driven lung cancer.* Sci Adv, 2022. **8**(39): p. eabo1123.
73. Relogio, A., Thomas, P., Medina-Perez, P., Reischl, S., Bervoets, S., Gloc, E., Riemer, P., Mang-Fatehi, S., Maier, B., Schafer, R., Leser, U., Herzel, H., Kramer, A., and Sers, C., *Ras-mediated deregulation of the circadian clock in cancer.* PLoS Genet, 2014. **10**(5): p. e1004338.
74. El-Athman, R., Genov, N.N., Mazuch, J., Zhang, K., Yu, Y., Fuhr, L., Abreu, M., Li, Y., Wallach, T., Kramer, A., Schmitt, C.A., and Relógio, A., *The Ink4a/Arf locus operates as a regulator of the circadian clock modulating RAS activity.* PLOS Biology, 2017. **15**(12): p. e2002940.
75. Liu, Z., Selby, C.P., Yang, Y., Lindsey-Boltz, L.A., Cao, X., Eynullazada, K., and Sancar, A., *Circadian regulation of c-MYC in mice.* Proc Natl Acad Sci U S A, 2020. **117**(35): p. 21609-21617.
76. Huber, A.L., Papp, S.J., Chan, A.B., Henriksson, E., Jordan, S.D., Kriebs, A., Nguyen, M., Wallace, M., Li, Z., Metallo, C.M., and Lamia, K.A., *CRY2 and FBXL3 Cooperatively Degrade c-MYC.* Mol Cell, 2016. **64**(4): p. 774-789.

77. Fu, L., Pelicano, H., Liu, J., Huang, P., and Lee, C., *The circadian gene Period2 plays an important role in tumor suppression and DNA damage response in vivo.* Cell, 2002. **111**(1): p. 41-50.
78. Dong, Z., et al., *Targeting Glioblastoma Stem Cells through Disruption of the Circadian Clock.* Cancer Discov, 2019. **9**(11): p. 1556-1573.
79. Puram, R.V., Kowalczyk, M.S., de Boer, C.G., Schneider, R.K., Miller, P.G., McConkey, M., Tothova, Z., Tejero, H., Heckl, D., Jaras, M., Chen, M.C., Li, H., Tamayo, A., Cowley, G.S., Rozenblatt-Rosen, O., Al-Shahrour, F., Regev, A., and Ebert, B.L., *Core Circadian Clock Genes Regulate Leukemia Stem Cells in AML.* Cell, 2016. **165**(2): p. 303-16.
80. Papagiannakis, A., Niebel, B., Wit, E.C., and Heinemann, M., *Autonomous Metabolic Oscillations Robustly Gate the Early and Late Cell Cycle.* Molecular Cell, 2017. **65**(2): p. 285-295.
81. Ahn, E., Kumar, P., Mukha, D., Tzur, A., and Shlomi, T., *Temporal fluxomics reveals oscillations in TCA cycle flux throughout the mammalian cell cycle.* Molecular systems biology, 2017. **13**(11): p. 953.
82. Panda, S., Banerjee, N., and Chatterjee, S., *Solute carrier proteins and c-Myc: a strong connection in cancer progression*, in *Drug Discovery Today*. 2020, Elsevier Ltd. p. 891-900.
83. Elorza, A., Soro-Arnaiz, I., Melendez-Rodriguez, F., Rodriguez-Vaello, V., Marsboom, G., de Carcer, G., Acosta-Iborra, B., Albacete-Albacete, L., Ordonez, A., Serrano-Oviedo, L., Gimenez-Bachs, J.M., Vara-Vega, A., Salinas, A., Sanchez-Prieto, R., Martin del Rio, R., Sanchez-Madrid, F., Malumbres, M., Landazuri, M.O., and Aragones, J., *HIF2alpha acts as an mTORC1 activator through the amino acid carrier SLC7A5.* Mol Cell, 2012. **48**(5): p. 681-91.
84. Cormerais, Y., Giuliano, S., LeFloch, R., Front, B., Durivault, J., Tambutte, E., Massard, P.A., de la Ballina, L.R., Endou, H., Wempe, M.F., Palacin, M., Parks, S.K., and Pouyssegur, J., *Genetic Disruption of the Multifunctional CD98/LAT1 Complex Demonstrates the Key Role of Essential Amino Acid Transport in the Control of mTORC1 and Tumor Growth.* Cancer Res, 2016. **76**(15): p. 4481-92.
85. Yue, M., Jiang, J., Gao, P., Liu, H., and Qing, G., *Oncogenic MYC Activates a Feedforward Regulatory Loop Promoting Essential Amino Acid Metabolism and Tumorigenesis.* Cell reports, 2017. **21**(13): p. 3819-3832.
86. Hayashi, K., Jutabha, P., Endou, H., and Anzai, N., *c-Myc is crucial for the expression of LAT1 in MIA Paca-2 human pancreatic cancer cells.* Oncology reports, 2012. **28**(3): p. 862-6.
87. Venkateswaran, N., Lafita-Navarro, M.C., Hao, Y.H., Kilgore, J.A., Perez-Castro, L., Braverman, J., Borenstein-Auerbach, N., Kim, M., Lesner, N.P., Mishra, P., Brabletz, T., Shay, J.W., DeBerardinis, R.J., Williams, N.S., Yilmaz, O.H., and Conacci-Sorrell, M., *MYC promotes tryptophan uptake and metabolism by the kynurenine pathway in colon cancer.* Genes Dev, 2019. **33**(17-18): p. 1236-1251.
88. Pathria, G., Verma, S., Yin, J., Scott, D.A., and Ronai, Z.A., *MAPK signaling regulates c-MYC for melanoma cell adaptation to asparagine restriction.* EMBO reports, 2021. **22**(3): p. e51436.
89. Gamble, L.D., et al., *Inhibition of polyamine synthesis and uptake reduces tumor progression and prolongs survival in mouse models of neuroblastoma.* Science Translational Medicine, 2019. **11**(477): p. eaau1099.
90. Wang, R., Dillon, C.P., Shi, L.Z., Milasta, S., Carter, R., Finkelstein, D., McCormick, L.L., Fitzgerald, P., Chi, H., Munger, J., and Green, D.R., *The transcription factor Myc controls metabolic reprogramming upon T lymphocyte activation.* Immunity, 2011. **35**(6): p. 871-82.
91. Wang, H., Wang, F., Ouyang, W., Jiang, X., and Wang, Y., *BCAT1 overexpression regulates proliferation and c-Myc/GLUT1 signaling in head and neck squamous cell carcinoma.* Oncology reports, 2021. **45**(5).
92. Yan, Q.Y., Lu, Y.T., Zhou, L.L., Chen, J.L., Xu, H.J., Cai, M.J., Shi, Y., Jiang, J.G., Xiong, W.Y., Gao, J., and Wang, H.D., *Mechanistic insights into GLUT1 activation and clustering revealed by super-resolution imaging.* P Natl Acad Sci USA, 2018. **115**(27): p. 7033-7038.
93. Selfridge, J.M., Gotoh, T., Schiffhauer, S., Liu, J., Stauffer, P.E., Li, A., Capelluto, D.G., and Finkielstein, C.V., *Chronotherapy: Intuitive, Sound, Founded...But Not Broadly Applied.* Drugs, 2016.
94. Ushmorov, A., Hogarty, M.D., Liu, X., Knauss, H., Debatin, K.M., and Beltinger, C., *N-myc augments death and attenuates protective effects of Bcl-2 in trophically stressed neuroblastoma cells.* Oncogene, 2008. **27**(24): p. 3424-34.
95. Valentijn, L.J., Koppen, A., van Asperen, R., Root, H.A., Haneveld, F., and Versteeg, R., *Inhibition of a new differentiation pathway in neuroblastoma by copy number defects of N-myc, Cdc42, and nm23 genes.* Cancer Res, 2005. **65**(8): p. 3136-45.

96. Patro, R., Duggal, G., Love, M.I., Irizarry, R.A., and Kingsford, C., *Salmon provides fast and bias-aware quantification of transcript expression.* Nature methods, 2017. **14**(4): p. 417-419.
97. Soneson, C., Love, M.I., and Robinson, M.D., *Differential analyses for RNA-seq: transcript-level estimates improve gene-level inferences.* F1000Research, 2015. **4**: p. 1521-1521.
98. Bligh, E.G. and Dyer, W.J., *A rapid method of total lipid extraction and purification.* Canadian journal of biochemistry and physiology, 1959. **37**(8): p. 911-7.
99. Tambellini, N.P., Zaremberg, V., Turner, R.J., and Weljie, A.M., *Evaluation of extraction protocols for simultaneous polar and non-polar yeast metabolite analysis using multivariate projection methods.* Metabolites, 2013. **3**(3): p. 592-605.
100. Malik, D.M., Rhoades, S.D., and Weljie, A.M., *Extraction and Analysis of Pan-metabolome Polar Metabolites by Ultra Performance Liquid Chromatography–Tandem Mass Spectrometry (UPLC-MS/MS).* Bio-protocol, 2018. **8**(3): p. e2715.
101. Rhoades, S.D. and Weljie, A.M., *Comprehensive optimization of LC–MS metabolomics methods using design of experiments (COLMeD).* Metabolomics, 2016. **12**(12): p. 183.
102. Zhu, A., Ibrahim, J.G., and Love, M.I., *Heavy-tailed prior distributions for sequence count data: removing the noise and preserving large differences.* Bioinformatics, 2019. **35**(12): p. 2084-2092.
103. Pang, Z., Chong, J., Zhou, G., de Lima Morais, D.A., Chang, L., Barrette, M., Gauthier, C., Jacques, P.-É., Li, S., and Xia, J., *MetaboAnalyst 5.0: narrowing the gap between raw spectra and functional insights.* Nucleic Acids Research, 2021. **49**(W1): p. W388-W396.
104. Kanehisa, M., *KEGG Bioinformatics Resource for Plant Genomics and Metabolomics*, in *Plant Bioinformatics: Methods and Protocols*, D. Edwards, Editor. 2016, Springer New York: New York, NY. p. 55-70.
105. Nuñez, J.R., Anderton, C.R., and Renslow, R.S., *Optimizing colormaps with consideration for color vision deficiency to enable accurate interpretation of scientific data.* PLOS ONE, 2018. **13**(7): p. e0199239.

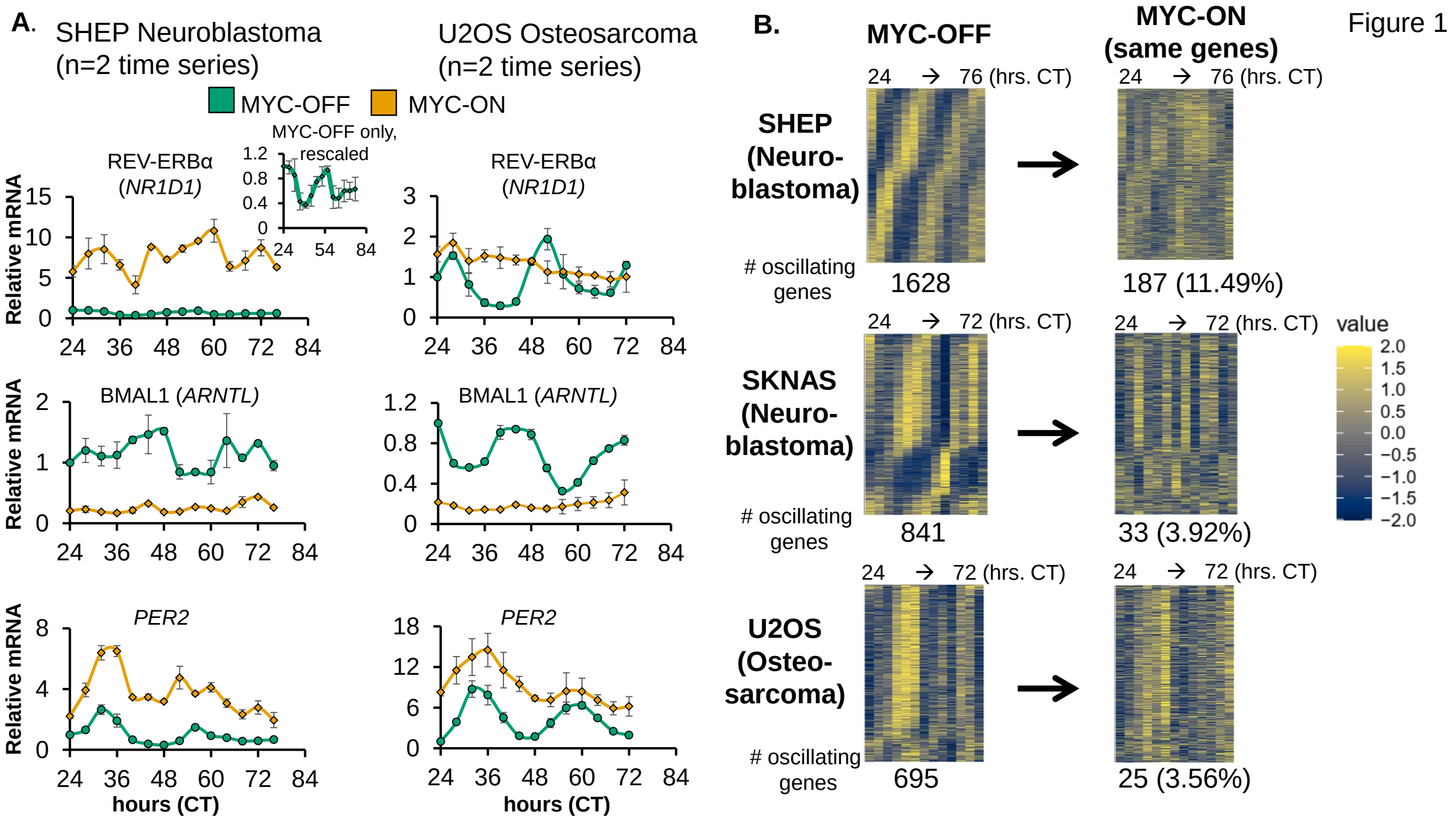
A.
SHEP Neuroblastoma
(n=2 time series)
U2OS Osteosarcoma
(n=2 time series)
MYC-OFF
MYC-ON
MYC-OFF only, rescaled
REV-ERBα (NR1D1)
BMAL1 (ARNTL)
PER2
Relative mRNA
hours (CT)
B.
MYC-OFF
MYC-ON (same genes)
24 → 76 (hrs. CT)
24 → 72 (hrs. CT)
SHEP (Neuro-blastoma)
SKNAS (Neuro-blastoma)
U2OS (Osteo-sarcoma)
oscillating genes
1628
187 (11.49%)
841
33 (3.92%)
695
25 (3.56%)
value

A.

MYC-OFF

MYC-ON

SHEP

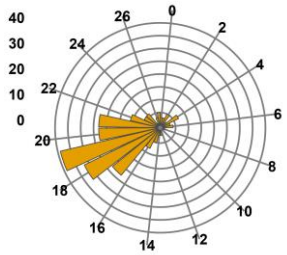

311 sets

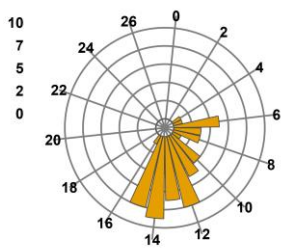

56 sets

SKNAS

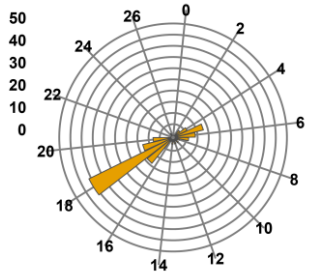

122 sets

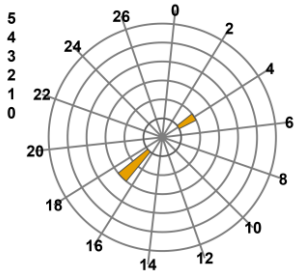

3 sets

U2OS

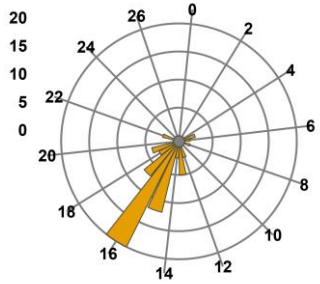

61 sets

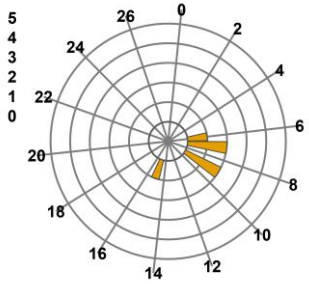

6 sets

B.

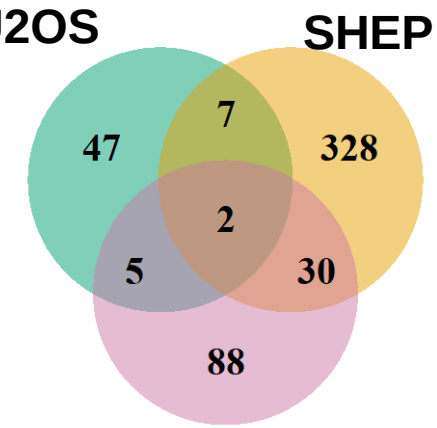

U2OS and SHEP

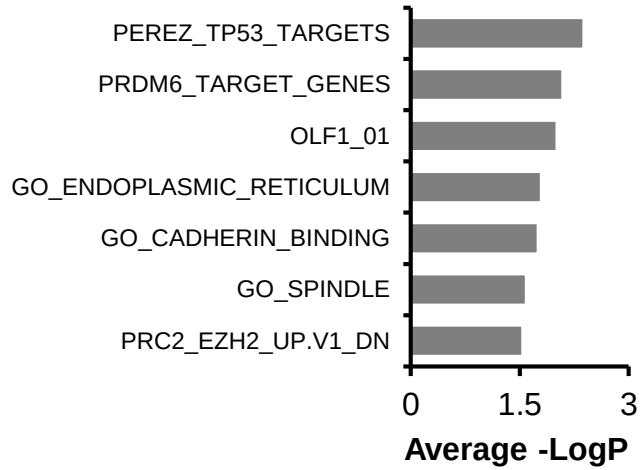

U2OS and SKNAS

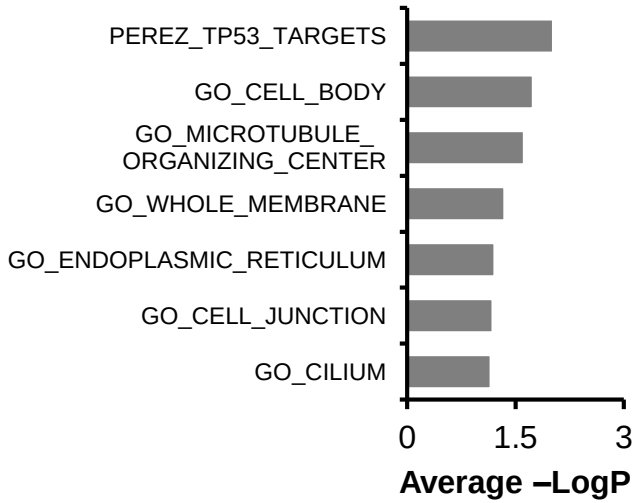

SHEP and SKNAS

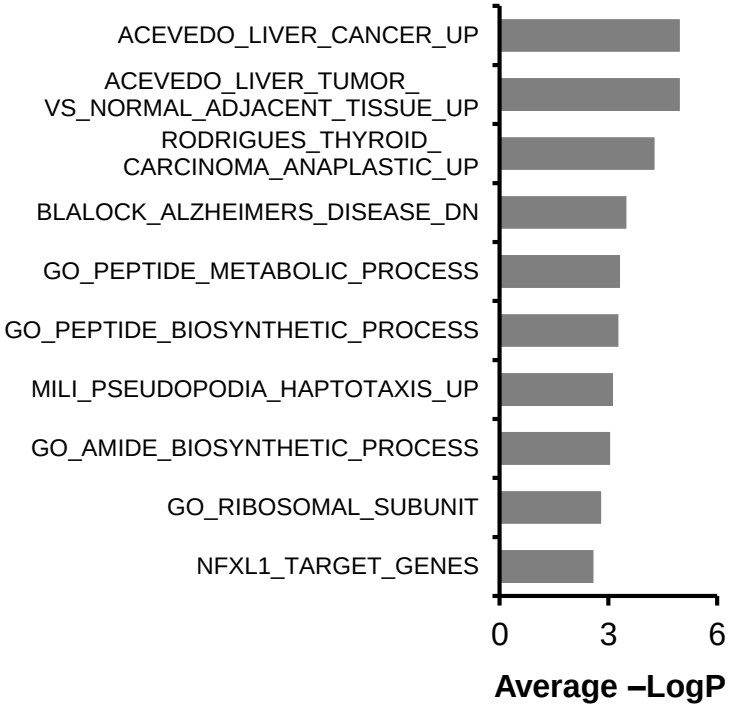

3 Cell Lines

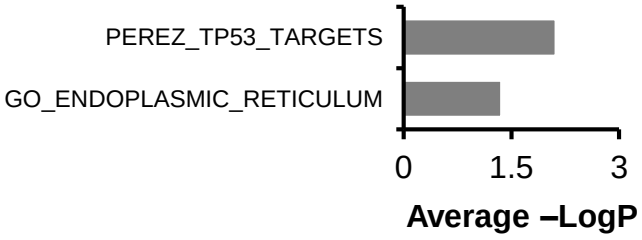

A.

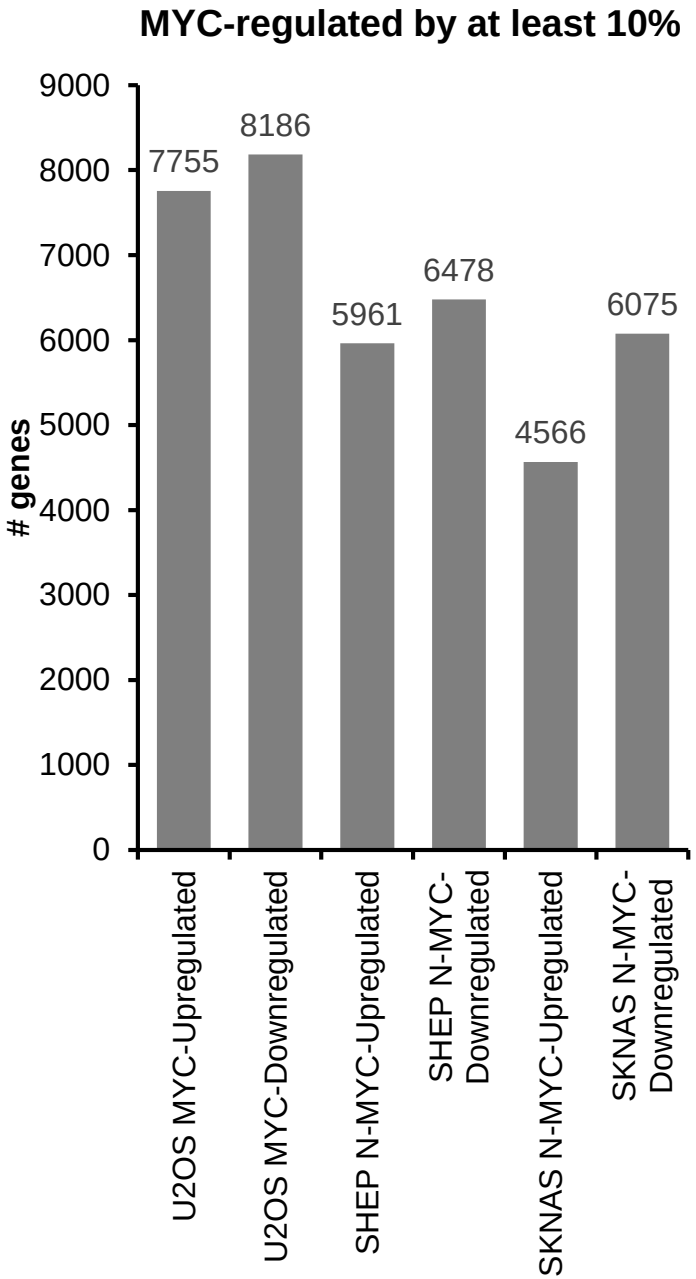
MYC-regulated by at least 10%
genes
9000
8000
7000
6000
5000
4000
3000
2000
1000
0
7755
8186
5961
6478
4566
6075
U2OS MYC-Upregulated
U2OS MYC-Downregulated
SHEP N-MYC-Upregulated
SHEP N-MYC-Downregulated
SKNAS N-MYC-Upregulated
SKNAS N-MYC-Downregulated

B.

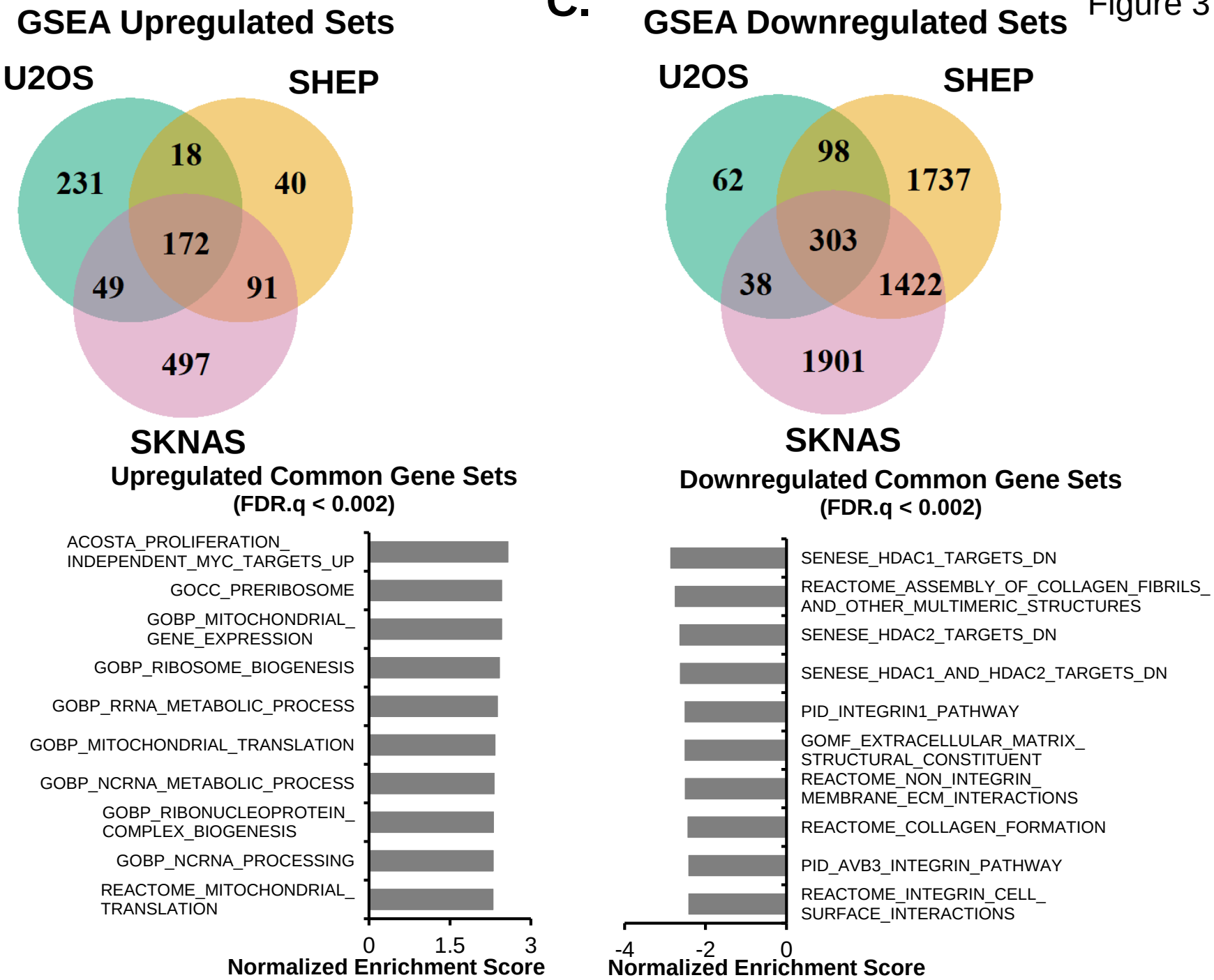
GSEA Upregulated Sets
U2OS
SHEP
231
18
40
172
49
91
497
SKNAS
Upregulated Common Gene Sets
(FDR.q < 0.002)
ACOSTA_PROLIFERATION_INDEPENDENT_MYC_TARGETS_UP
GOCC_PRERIBOSOME
GOBP_MITOCHONDRIAL_GENE_EXPRESSION
GOBP_RIBOSOME_BIOGENESIS
GOBP_RRNA_METABOLIC_PROCESS
GOBP_MITOCHONDRIAL_TRANSLATION
GOBP_NCRNA_METABOLIC_PROCESS
GOBP_RIBONUCLEOPROTEIN_COMPLEX_BIOGENESIS
GOBP_NCRNA_PROCESSING
REACTOME_MITOCHONDRIAL_TRANSLATION
0
1.5
3
Normalized Enrichment Score

C.

GSEA Downregulated Sets
U2OS
SHEP
62
98
1737
303
38
1422
1901
SKNAS
Downregulated Common Gene Sets
(FDR.q < 0.002)
SENESE_HDAC1_TARGETS_DN
REACTOME_ASSEMBLY_OF_COLLAGEN_FIBRILS_AND_OTHER_MULTIMERIC_STRUCTURES
SENESE_HDAC2_TARGETS_DN
SENESE_HDAC1_AND_HDAC2_TARGETS_DN
PID_INTEGRIN1_PATHWAY
GOMF_EXTRACELLULAR_MATRIX_STRUCTURAL_CONSTITUENT
REACTOME_NON_INTEGRIN_MEMBRANE_ECM_INTERACTIONS
REACTOME_COLLAGEN_FORMATION
PID_AVB3_INTEGRIN_PATHWAY
REACTOME_INTEGRIN_CELL_SURFACE_INTERACTIONS
-4
-2
0
Normalized Enrichment Score

A.

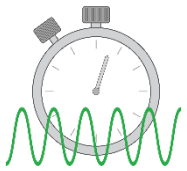

PSEA pathways that oscillate in MYC-OFF

MYC

Formerly oscillating pathways (PSEA) become **upregulated (GSEA)** in **MYC-ON**

or

Formerly oscillating pathways (PSEA) become **downregulated (GSEA)** in **MYC-ON**

B.

SHEP

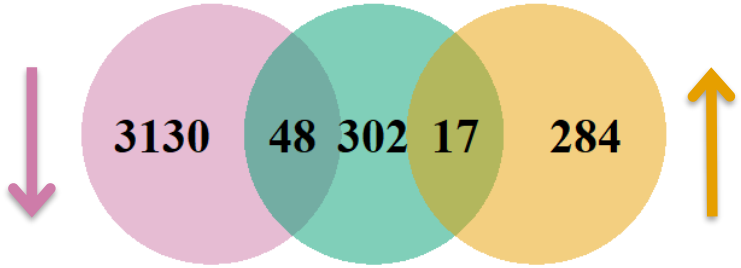

Oscillating to downregulated
(FDR.q = 0)

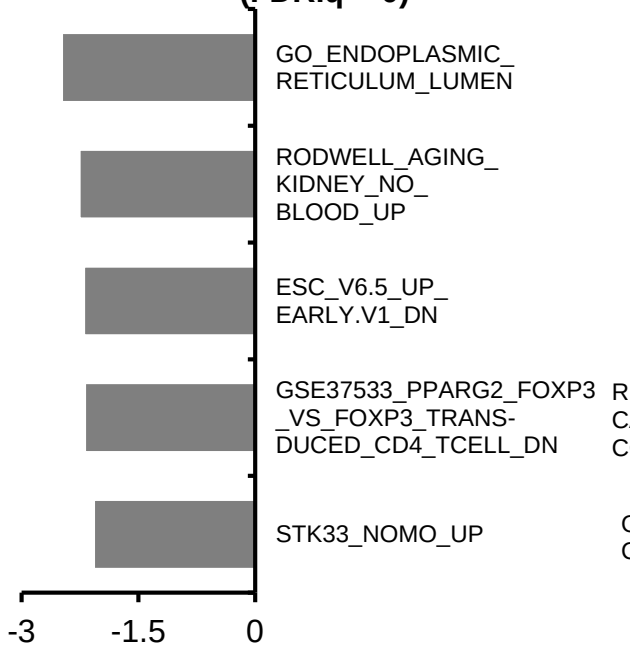

Oscillating to upregulated
(FDR.q = 0)

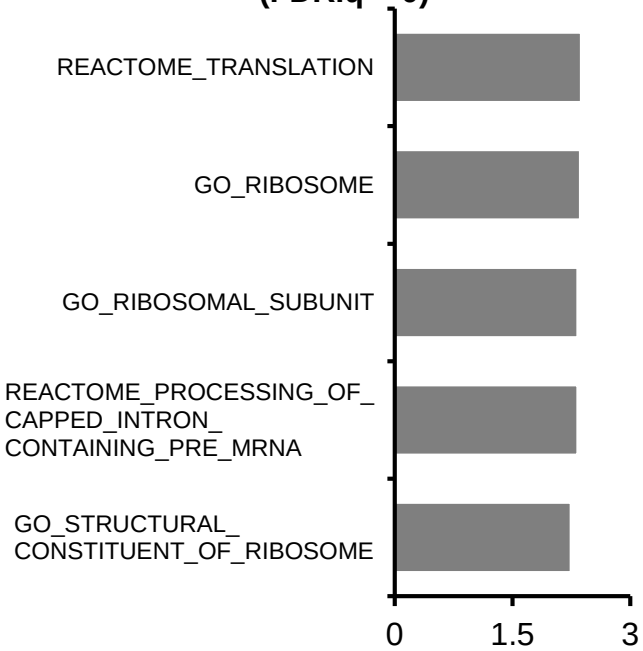

C.

SKNAS

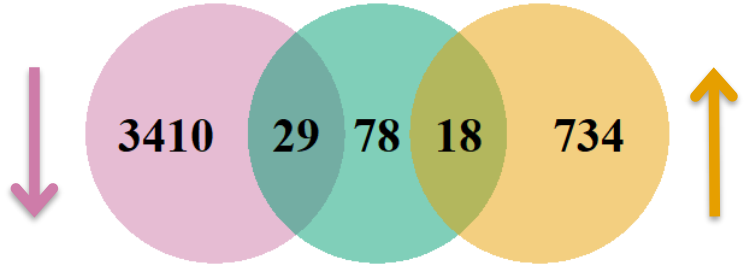

Oscillating to downregulated
(FDR.Q < 0.051)

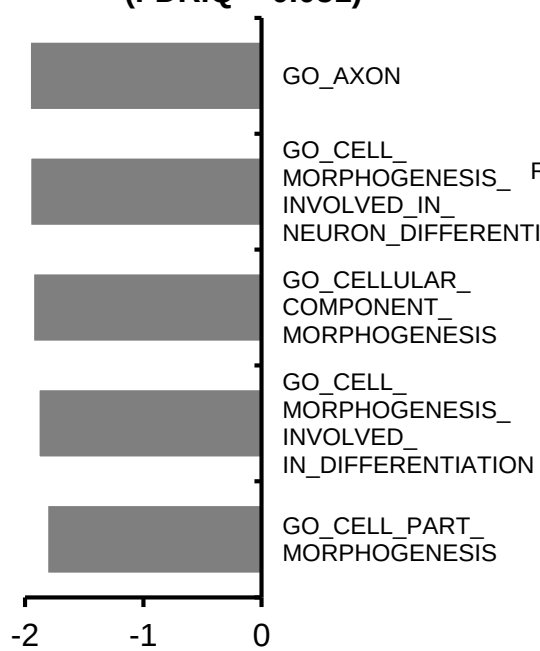

Oscillating to upregulated
(FDR.q = 0)

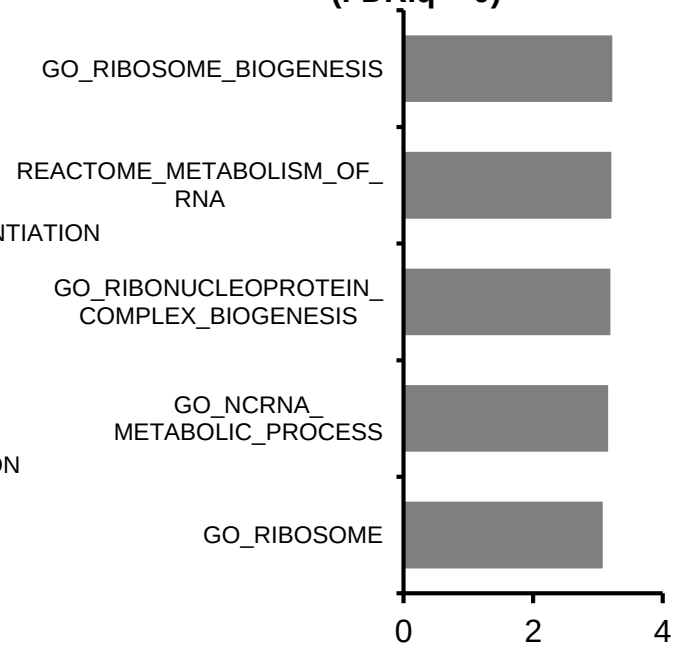

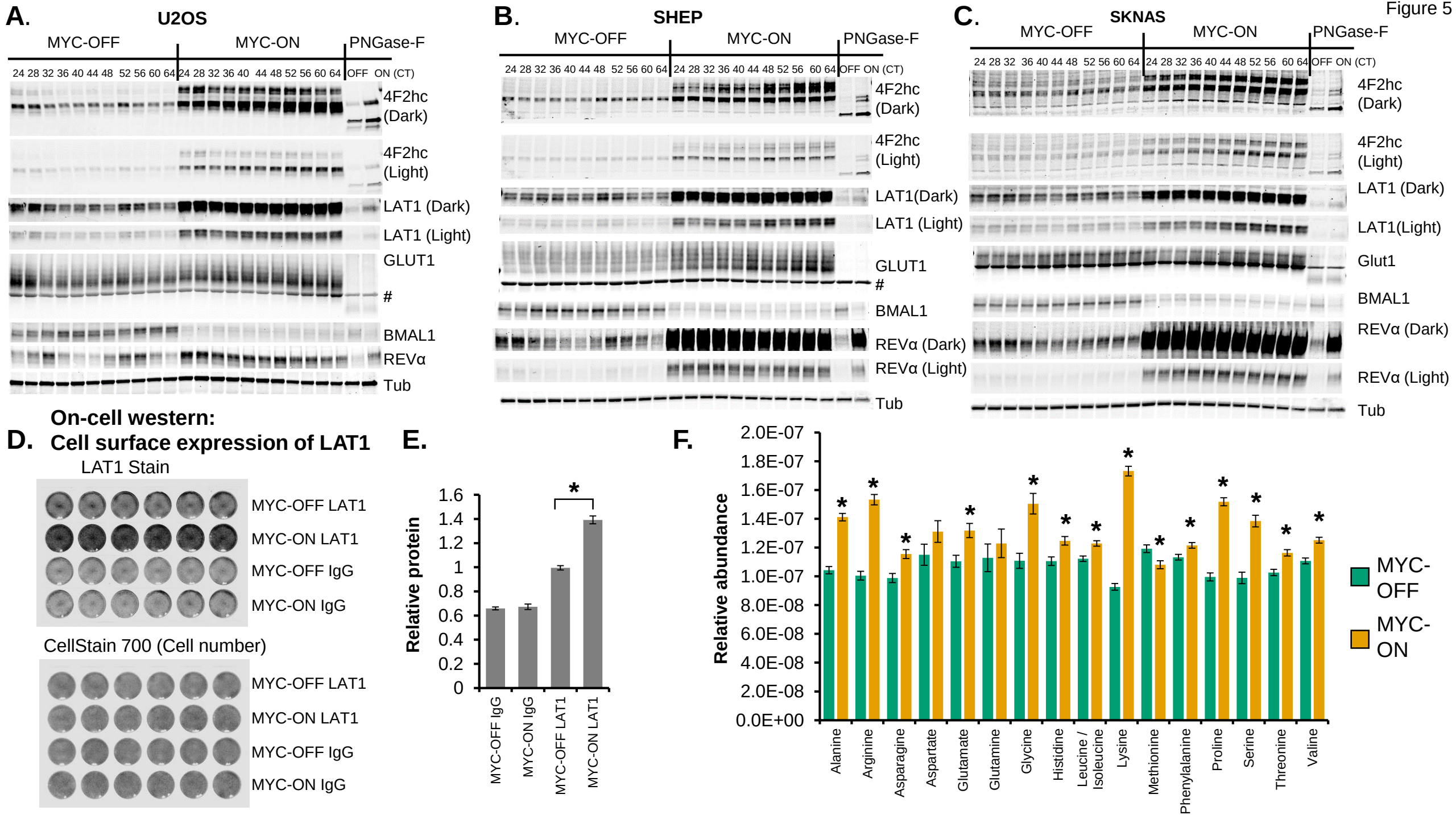
A.
U2OS
MYC-OFF
MYC-ON
PNGase-F
24 28 32 36 40 44 48 52 56 60 64 24 28 32 36 40 44 48 52 56 60 64 OFF ON (CT)
4F2hc (Dark)
4F2hc (Light)
LAT1 (Dark)
LAT1 (Light)
GLUT1
#
BMAL1
REVα
Tub
B.
SHEP
MYC-OFF
MYC-ON
PNGase-F
24 28 32 36 40 44 48 52 56 60 64 24 28 32 36 40 44 48 52 56 60 64 OFF ON (CT)
4F2hc (Dark)
4F2hc (Light)
LAT1(Dark)
LAT1 (Light)
GLUT1
#
BMAL1
REVα (Dark)
REVα (Light)
Tub
C.
SKNAS
MYC-OFF
MYC-ON
PNGase-F
24 28 32 36 40 44 48 52 56 60 64 24 28 32 36 40 44 48 52 56 60 64 OFF ON (CT)
4F2hc (Dark)
4F2hc (Light)
LAT1 (Dark)
LAT1(Light)
Glut1
BMAL1
REVα (Dark)
REVα (Light)
Tub
D.
On-cell western:
Cell surface expression of LAT1
LAT1 Stain
MYC-OFF LAT1
MYC-ON LAT1
MYC-OFF IgG
MYC-ON IgG
CellStain 700 (Cell number)
MYC-OFF LAT1
MYC-ON LAT1
MYC-OFF IgG
MYC-ON IgG
E.
Relative protein
1.6
1.4
1.2
1
0.8
0.6
0.4
0.2
0
MYC-OFF IgG
MYC-ON IgG
MYC-OFF LAT1
MYC-ON LAT1
F.
Relative abundance
2.0E-07
1.8E-07
1.6E-07
1.4E-07
1.2E-07
1.0E-07
8.0E-08
6.0E-08
4.0E-08
2.0E-08
0.0E+00
Alanine
Arginine
Asparagine
Aspartate
Glutamate
Glutamine
Glycine
Histidine
Leucine / Isoleucine
Lysine
Methionine
Phenylalanine
Proline
Serine
Threonine
Valine
MYC-OFF
MYC-ON

A.

MYC-OFF

24 → 72

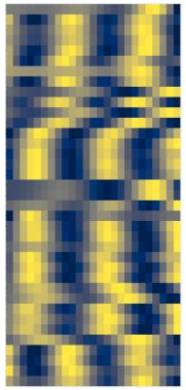

37

MYC-ON (same metabolites)

24 → 72 (hrs. CT)

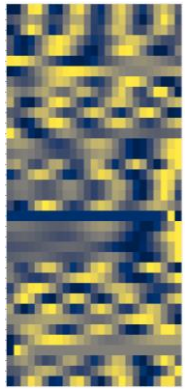

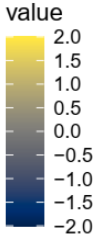

6 (16.22%)

oscillating metabolites

B.

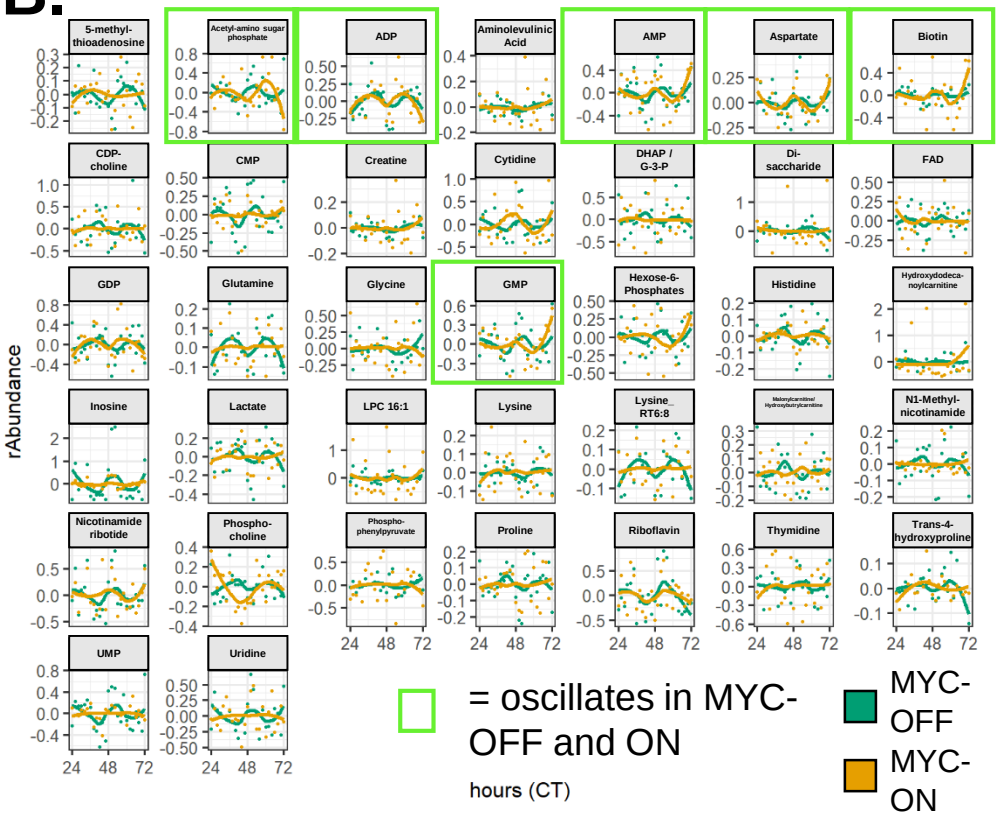

C.

KEGG Enrichment of Oscillating Metabolites P<0.05

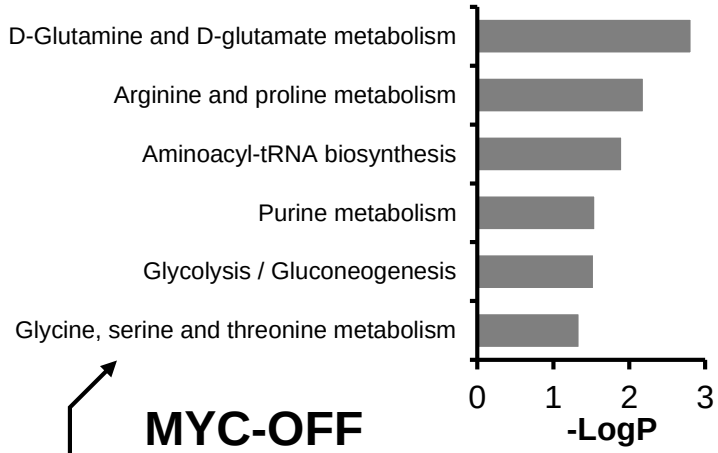

MYC-OFF

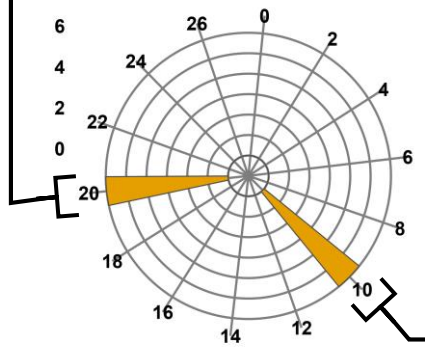

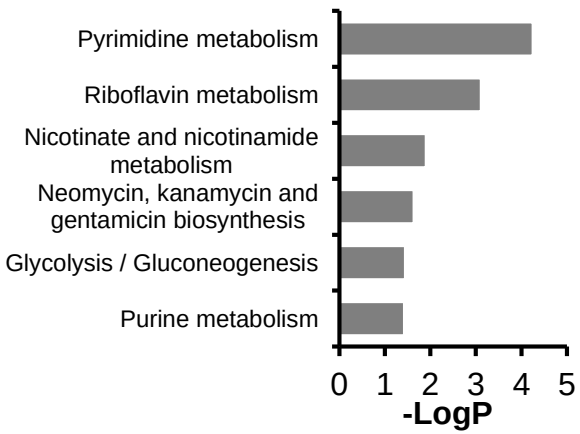

MYC-ON

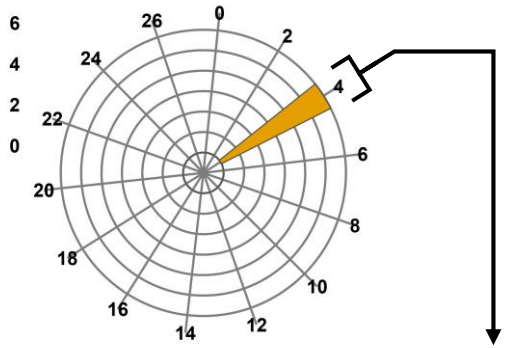

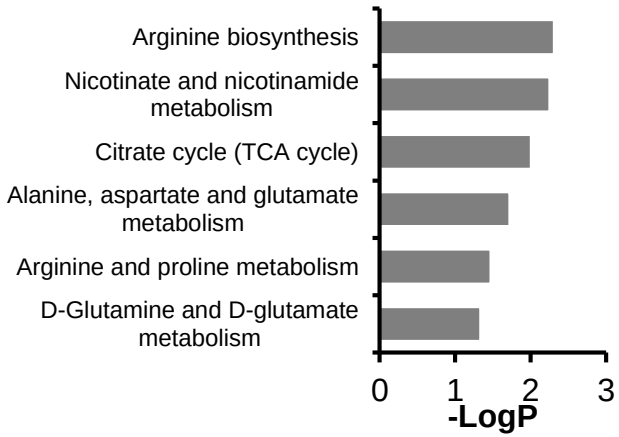

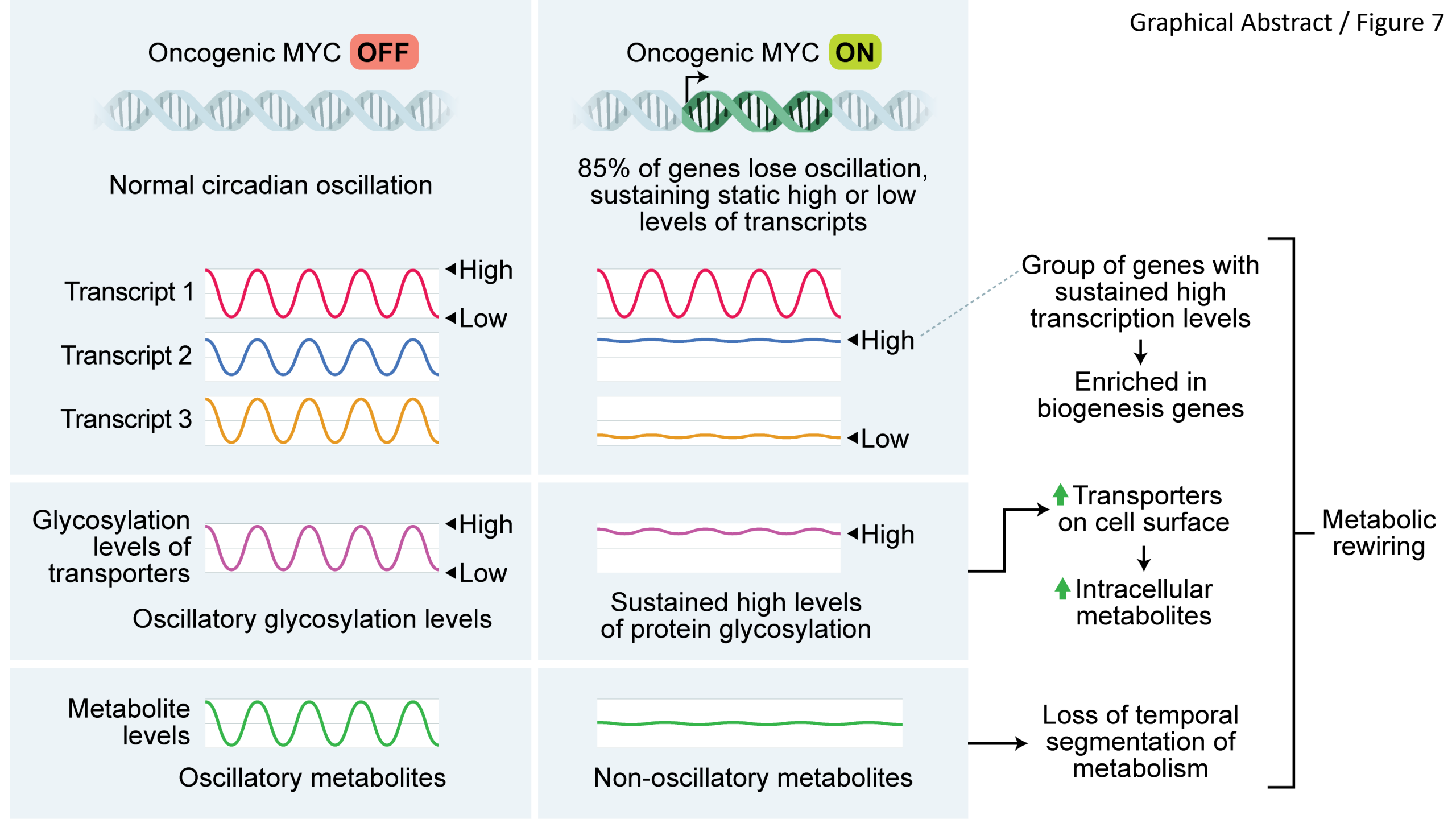
Oncogenic MYC OFF
Oncogenic MYC ON
Normal circadian oscillation
85% of genes lose oscillation, sustaining static high or low levels of transcripts
Transcript 1
Transcript 2
Transcript 3
High
Low
Group of genes with sustained high transcription levels
Enriched in biogenesis genes
Glycosylation levels of transporters
Oscillatory glycosylation levels
Sustained high levels of protein glycosylation
Transporters on cell surface
Intracellular metabolites
Metabolite levels
Oscillatory metabolites
Non-oscillatory metabolites
Loss of temporal segmentation of metabolism
Metabolic rewiring